Expert Systems With Applications 227 (2023) 120282

Contents lists available at ScienceDirect

Expert Systems With Applications

journal homepage: www.elsevier.com/locate/eswa

Automated breast cancer detection in mammography using ensemble classifier and feature weighting algorithms

Fei Yan [a,*], Hesheng Huang [a], Witold Pedrycz [b,c,d], Kaoru Hirota [e]

[a] School of Computer Science and Technology, Changchun University of Science and Technology, Changchun 130022, China
[b] Department of Electrical and Computer Engineering, University of Alberta, Edmonton T6G 2R3, Canada
[c] Systems Research Institute, Polish Academy of Sciences, Warsaw 00-901, Poland
[d] Department of Computer Engineering, Istinye University, Istanbul 34010, Turkey
[e] School of Computing, Tokyo Institute of Technology, Yokohama 226-8502, Japan

ARTICLE INFO

Keywords:
Computer-aided diagnosis
Breast cancer detection
Mammography
Ensemble classifier
Feature weighting

ABSTRACT

Breast cancer exhibits one of the highest incidence and mortality rates among all cancers affecting women. The early detection of breast cancer reduces mortality and is crucial for prolonging life expectancy. Although mammography is the most often used screening technique in clinical practice, previous studies reviewing mammograms diagnosed by radiologists have commonly revealed false negatives and false positives. Ongoing advances in machine learning techniques have triggered new motivation for the development of computer-aided diagnosis (CAD) systems, which could be applied to assist radiologists in improving final diagnostic accuracy. In this study, an automated methodology for detecting breast cancer in mammography images is proposed based on an ensemble classifier and feature weighting algorithms. First, a novel region extraction approach is proposed to constrain the search area for suspicious breast lesions and an original pectoral removal method is proposed to avoid interference when identifying a region of interest (ROI). In addition, an effective segmentation strategy is developed to automatically identify ROIs whose textural and morphological features are then fused and weighted to generate new feature vectors using a feature weighting algorithm. Finally, an ensemble classifier model is designed using k-nearest neighbor (KNN), bagging, and eigenvalue classification (EigenClass) to determine whether a mammogram contains normal, benign, or malignant tumors based on a majority voting rule. A series of experiments was conducted using the Digital Database for Screening Mammography (DDSM) and Mammographic Image Analysis Society (MIAS) datasets, the results of which demonstrated the proposed scheme outperformed comparable algorithms.

1. Introduction

Cancer may surpass cardiovascular disease as the leading cause of premature death in most countries worldwide, according to World Health Organization data collected in 2019 from 183 countries (Bray, Laversanne, Weiderpass, & Soerjomataram, 2021). Compared with lung, colorectal, prostate, and stomach cancers, female breast cancer ranks as the most commonly diagnosed cancer by GLOBOCAN 2020 estimates of cancer incidence and mortality, produced by the International Agency for Research on Cancer (Sung et al., 2021). Early detection can reduce breast cancer mortality (Althobaiti et al., 2022; Lotter et al., 2021; Ragab, Albukhari, Alyami, & Mansour, 2022), as it is crucial for timely treatment used to prolong life expectancy. Various medical imaging modalities, such as mammography, ultrasound, magnetic resonance (MR), and histological images, are used by radiologists for breast cancer diagnosis, though mammography is the most commonly used screening technique in clinical practice (Yassin, Omran, El Houby, & Allam, 2018). However, a recent review of mammograms diagnosed by radiologists revealed many false negatives (Hovda et al., 2022; Larsen et al., 2022). In order to address this issue, double reading is employed to decrease the occurrence of missed cancers (Han et al., 2017). However, double reading increases the workload for radiologists and is especially problematic given the scarcity of screening radiologists. Therefore, accurate early screening of breast cancer is a critical yet challenging task.

Advances in computer hardware and the ongoing expansion of machine learning technology has provided a motivation for the development of computer-aided diagnosis (CAD) systems. In recent years, CAD has been widely utilized for breast cancer detection, to assist and facilitate professional radiologists and improve the accuracy of

* Corresponding author at: School of Computer Science and Technology, Changchun University of Science and Technology, Changchun 130022, China.
E-mail addresses: yanfei@cust.edu.cn (F. Yan), hhs_cust@yeah.net (H. Huang), wpedrycz@ualberta.ca (W. Pedrycz), hirota@bit.edu.cn (K. Hirota).

https://doi.org/10.1016/j.eswa.2023.120282
Received 17 November 2022; Received in revised form 24 April 2023; Accepted 24 April 2023
Available online 29 April 2023

the diagnostic process (Aljuaid, Alturki, Alsubaie, Cavallaro, & Liotta, 2022; Assari, Mahloojifar, & Ahmadinejad, 2022; Maqsood, Damaševičius, & Maskeliūnas, 2022; Sechopoulos, Teuwen, & Mann, 2021; Zebari et al., 2021b). In addition, CAD has been considered as a second reading of breast cancer to enhance efficiency and reduce radiologist workloads (Li, Chen, Nailon, Davies, & Laurenson, 2021). However, in addition to the breast, mammograms often include noise, artifacts, and background objects that affect diagnostic results. It is thus critical to remove these obstacles to improve the accuracy of breast cancer screenings. Furthermore, the pixel intensity of the pectoral muscle is very similar to that of suspicious breast lesions, which makes it difficult to automatically locate and classify regions of interest (ROIs) in mammograms. As a result, several previous studies have investigated the removal of pectoral muscles from images, to reduce their interference (Girija & Sudheep, 2022; Moghbel, Ooi, Ismail, Hau, & Memari, 2020; Rampun, Morrow, Scotney, & Winder, 2017).

The primary steps in CAD systems using mammogram images for breast cancer detection include preprocessing, ROI segmentation, feature extraction and selection, and classification (Zebari et al., 2021a). Feature extraction is critical in the field of image classification and various techniques have been proposed in recent decades (Cao, Pang, Xie, Khan, & Shao, 2021). Generally, feature extraction algorithms can be classified as utilizing handcrafted or deep features. Deep learning-based approaches are becoming more popular due to better performance, but at the cost of increased complexity required for training, as measured by the runtime, computing power, and dataset size (Tripathi & Jalal, 2021). In addition, handcrafted features have been shown to outperform deep features for smaller sample sizes and with increased interpretability (Lin, Hasenstab, Moura Cunha, & Schwartzman, 2020). Therefore, traditional methods using handcrafted features (i.e., textural and morphological features) remain useful for breast cancer detection. Furthermore, ROI segmentation in mammograms involves two approaches: manual and automated delineation. The manual selection of ROI patches requires a professional radiologist to mark the lesion, which is a time-consuming and tedious task. As such, several studies have investigated the development of automated ROI segmentation methods for breast cancer detection and diagnosis, to improve the overall efficiency of CAD. However, many existing methods fail to segment ROIs with sufficient accuracy or precision.

In this study, an automated technique for detecting breast cancer in mammography images is proposed, based on an ensemble classifier and feature weighting algorithms, and used to classify suspicious lesions as normal, benign, or malignant tumors. In this process, a novel region extraction method is first proposed to distinguish the breast region in the mammogram. A pectoral muscle removal algorithm is also applied in the extracted breast region and an automated segmentation strategy is then developed to segment the ROI. The resulting textural and morphological features are determined and used to construct a feature vector that serves as the input to an ensemble classifier model. A feature weighting algorithm is also proposed to improve the classification performance of the model by assigning an optimal weight to each feature. In order to validate the effectiveness of the proposed scheme, a series of experiments were conducted using the Digital Database for Screening Mammography (DDSM) and Mammographic Image Analysis Society (MIAS) datasets. In summary, the primary contributions of this study are organized as follows:

(1) A novel breast region extraction technique is proposed based on image fusion and filtering methods, used to constrain the search area for suspicious lesions and enhance contrast in mammograms, thereby reducing false negative and false positive ratios for breast cancer detection.
(2) A pectoral muscle removal algorithm, applied in the mediolateral oblique (MLO) view of the mammogram, is proposed using adaptive local Otsu thresholding and morphological operations to reduce interference from the pectoral muscle for ROI segmentation and localization.
(3) An ROI segmentation strategy is proposed on the basis of dynamic thresholding and region growing algorithms and used to automatically locate, select, and segment ROIs to improve the efficiency of breast cancer detection.
(4) An improved INFO algorithm is proposed using an opposition-based learning method, which is employed to develop a feature weighting technique that assigns optimal weights to each feature extracted from ROIs, to further improve the accuracy of breast cancer detection.
(5) An ensemble classifier model is proposed by combining k-nearest neighbor (KNN), bagging, and eigenvalue classification (Eigen-Class) algorithms to predict whether a mammogram includes normal, benign, or malignant tumors using a majority voting rule, to effectively assist radiologists in detecting breast cancer.

The remainder of this article is organized as follows. Related works involving CAD systems for breast cancer diagnosis are systematically summarized in Section 2. Breast region extraction and pectoral muscle removal techniques are presented in Section 3. An automated ROI segmentation strategy for mammograms is formulated in Section 4. A breast cancer detection scheme is proposed in Section 5, based on ensemble classifier and feature weighting algorithms. Two common mammogram datasets are then used to validate the proposed scheme in Section 6, wherein the experimental results are further analyzed and discussed.

2. Literature review for breast cancer detection

Breast cancer exhibits one of the highest incidence and mortality rates among cancers affecting women around the world. The early detection of cancer can enable patients to receive timely treatment, which is essential to reducing cancer mortality. Ongoing advances in machine learning techniques have also triggered new motivation for the development of CAD systems. As such, several recent studies have investigated the development of CAD for assisting radiologists and improving diagnostic accuracy. A summary of these studies involving mammogram images is provided below.

In the early stages, Sharma et al. proposed a CAD system used to detect abnormalities or suspicious areas in mammograms (Sharma & Khanna, 2015). In this process, ROI patches were extracted manually from the breast region. The properties of Zernike moments were then used to analyze the textural features of ROI patches and a support vector machine (SVM) was applied to classify samples as malignant or non-malignant. However, Zernike moments suffer from high computational complexity, particularly in the case of higher-order moments. To overcome this deficiency, Singh et al. proposed an improved CAD system for the classification of benign and malignant breast tissues, in which the properties of generalized pseudo-Zernike moments were used as texture descriptors for ROIs (Singh & Urooj, 2016). In this process, ROI patches were first manually extracted from mammograms and an improved classifier (i.e., an adaptive differential evolution wavelet neural network) was then proposed to improve the classification accuracy of the CAD system. However, the manual segmentation of ROI patches is usually time-consuming and tedious.

To improve overall CAD efficiency, Tsochatzidis et al. proposed a content-based image retrieval algorithm used to diagnose mammographic masses (Tsochatzidis et al., 2017). A semi-automated segmentation method based on dynamic programming was then applied to acquire a contour delineation of the mass. Shape and textural features were also extracted from the segmented mass regions, which were transformed by a set of SVMs into a new representation vector. The average accuracy of this scheme in discriminating between benign and malignant masses was 81.00% for DDSM data. In addition, Chakraborty et al. proposed a novel strategy for the automated detection and diagnosis of masses in mammograms (Chakraborty, Midya, & Rabidas, 2018). An iterative method for multilevel high-to-low intensity thresholding,

controlled by radial region growing, was applied for the detection of masses. Naive Bayes (NB) and Random Forest (RF) classifiers have also been employed for mass classification. The performance of this approach was evaluated using images from the DDSM dataset. The diagnostic accuracy achieved by RF and NB models for benign and malignant masses was 77.89% and 72.79%, respectively. Automated segmentation improved the overall efficiency, at the expense of lower accuracy.

To enhance the accuracy of breast cancer diagnosis, Heidari et al. proposed a new CAD scheme based on the analysis of global mammographic image features, extracting three feature subgroups from spatial and frequency domains (Heidari et al., 2019). An SVM was then used to predict the likelihood of individual cases being malignant, which yielded a prediction accuracy of 92%. However, this approach has several limitations, as it does not consider the identification or selection of optimal features. High-dimensional data features also increase computational costs significantly and reduce the classification performance of machine learning algorithms. In contrast, deep learning is a promising technique that addresses the high dimensionality and low accuracy of manual features. For example, Escorcia-Gutierrez et al. proposed an automated deep learning based breast cancer diagnosis model using digital mammograms (Escorcia-Gutierrez et al., 2022). In this model, a deep convolutional neural network-based Residual Network (ResNet34) was applied for feature extraction, in which the hyperparameters of a ResNet34 model were optimized using a chimp optimization algorithm. Finally, the wavelet neural network was employed to determine whether the mammograms were normal or abnormal. However, as discussed in (Shen, Wang, Gou, & Wang, 2020), deep learning models require large amounts of annotated training data to reduce the negative influence of overfitting, which can be difficult when considering patient privacy.

In order to solve the problem of overfitting in deep learning models used for breast cancer detection, data augmentation techniques have been introduced to expand the training data. Mahmood et al. proposed a novel deep learning-based convolutional neural network for detecting and classifying benign and malignant masses using mammogram images (Mahmood et al., 2022). In this process, transfer learning paradigms were used to enhance the pre-trained model by fine-tuning hyperparameters and a data augmentation technique was used to help overcome dataset size bottlenecks and mitigate overfitting. This scheme offered high performance for the automated classification of suspicious regions into benign and malignant classes. However, compared with such CAD schemes, multi-classification (i.e., normal, benign, and malignant) is more advantageous for helping radiologists diagnose breast cancer. Soulami et al. proposed an automated method for breast mass detection in mammograms, based on a capsule deep learning strategy, to classify breast lesions as normal, benign, and malignant (Soulami, Kaabouch, & Saidi, 2022). The proposed capsule network (CapsNet) was fine-tuned according to the number of kernels and capsules. Data augmentation techniques have also been used to expand the sizes of training samples and help the model generalize learned weights to new mammograms. The average accuracy of this multi-classification process for breast masses reached 77.78% and 62.50% for DDSM and INbreast data, respectively. It is apparent that multi-classification in breast cancer detection is still challenging, especially in improving the accuracy.

As discussed above, several issues remain in breast cancer detection algorithms utilizing mammogram images. As such, this study proposes a novel methodology for detecting breast cancer, based on ensemble classifier and feature weighting algorithms used to classify suspicious lesions as normal, benign, or malignant tumors. According to the contributions highlighted earlier, details of this proposed methodology are described in the following sections.

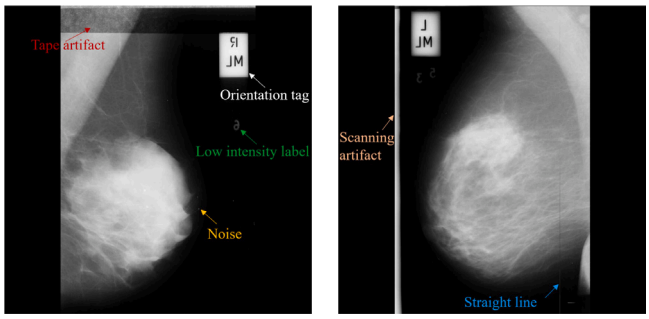

Fig. 1. A sample mammogram, illustrating the presence of noise and artifacts common in such images.

3. Region extraction and pectoral muscle removal

Mammograms are X-ray images that are widely used to detect early breast cancer. However, the backgrounds of mammograms often contain artifacts, noise, and insignificant objects such as labels, orientation tags, or scanning and tape artifacts (Mustra, Grgic, & Rangayyan, 2016), as shown in Fig. 1. These objects can negatively influence the CAD process and the search for suspicious lesions. In addition, such issues may also affect the determination of breast orientation (i.e., left or right breast) during disease diagnosis. Breast regions in mammograms must then be isolated to remove noise and non-significant objects, thereby constraining the search region. In this study, a novel region extraction method is first proposed using image fusion and filtering algorithms. Furthermore, the pectoral muscle in mammograms is highly similar to abnormal breast tissue and glandular parenchyma. Pectoral muscle removal from the breast region is therefore essential to the accurate localization and segmentation of ROIs. As such, an accurate and effective pectoral muscle removal approach is proposed based on adaptive local Otsu thresholding and morphological operations.

3.1. Region extraction based on image fusion and filtering techniques

Breast regions extracted from mammograms should not only include detailed contour information but also exhibit high fidelity to improve breast cancer screenings. Images acquired using pixel-level fusion offer more detailed information, the contrast of which can be enhanced using spatial filtering. An effective region extraction method is thus proposed. Specifically, a framework for this method is presented in Fig. 2, with steps described in detail as follows.

Step 1: Grayscale images in 12-bit and 16-bit formats were uniformly converted to an 8-bit format to reduce computational costs and facilitate breast abnormality detection (Duarte et al., 2015). Specifically, if the maximum pixel value in a mammogram is greater than 255, the image should be converted into an 8-bit grayscale format as follows:

$$\beta_{ij} = \sum_{i=1}^{m}\sum_{j=1}^{n} \frac{\alpha_{ij}}{65535} \times 255, \tag{1}$$

where m and n indicate the row and column sizes for the image format needing to be converted, α_{ij} is a pixel in the ith row and jth column, and β_{ij} represents the converted α_{ij} pixel.

Step 2: High-intensity pixel values outside the breast region are typically considered to be artificially generated noise, whose pixel values should be consistent with the background of the mammogram to facilitate subsequent breast region extraction. In addition, filtering techniques can be applied to the image to increase its quality, as weighted median filtering is often employed to smooth the image, average filtering is utilized to remove digital noise, and sharpening is used

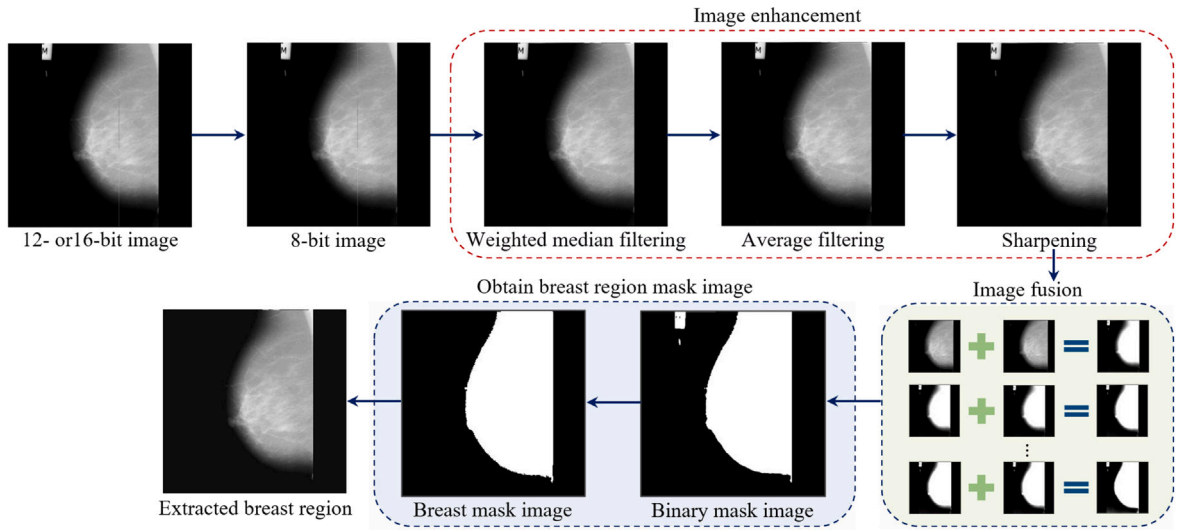

Fig. 2. A framework for the region extraction method based on image fusion and filtering techniques.

to enhance contrast, where the size of the filtering window is 3 × 3. Meanwhile, filtering techniques can be used to reduce discrepancies in lighting and exposure levels for mammogram images.

Step 3: The enhanced image from Step 2 is fused with itself multiple times using a pixel-level fusion strategy that emphasize the breast region over other unimportant objects. The specific image fusion employed here can be expressed as:

$$\lambda_{ij} = \begin{cases} \sum_{i=1}^{m}\sum_{j=1}^{n}\left(\lambda_{1_{ij}} + \lambda_{1_{ij}}\right) & \text{if } \lambda_{1_{ij}} < 255 \\ 255 & Otherwise \end{cases}, \tag{2}$$

where λ_{ij} denotes a pixel in the fused result, m and n are respectively the row and column sizes of the enhanced image, and $\lambda_{1_{ij}}$ represents the pixel to be fused.

Step 4: The fused image acquired in Step 3 is used to generate a mask (i.e., a binary image) of the mammogram as follows:

$$\gamma = \sum_{i=1}^{m}\sum_{j=1}^{n}\gamma_{ij} = \begin{cases} 1 & \text{if } \lambda_{ij} = 255 \\ 0 & Otherwise \end{cases}, \tag{3}$$

where γ is the acquired mask, m and n denote the row and column sizes of the fused image, respectively, and γ_{ij} is a pixel in the mask.

Step 5: The area of each connected component can be separately calculated from the mask obtained in Step 4. In this way, a mask of the breast region can be identified from the connected components with the largest areas. Pixels in other regions of the mammogram are then substituted with pixels whose values are close to the background.

To summarize, the proposed breast region extraction method, based on image fusion and filtering techniques, is used to remove noise and other unimportant objects to isolate and enhance the breast region in the original image.

3.2. Pectoral muscle removal based on adaptive local thresholding and morphological operations

Mammograms can typically be divided into MLO and Cranio-Caudal (CC) views (see Section 6). The pectoral muscle is generally discovered in the upper-right or upper-left area of MLO mammograms. As such, the left breast may be flipped horizontally to reduce the computational burden and facilitate pectoral muscle removal. Since a computer cannot automatically distinguish breast orientation (i.e., left or right), it becomes necessary to determine orientation in the MLO view prior to pectoral muscle removal. To address this issue, an effective breast

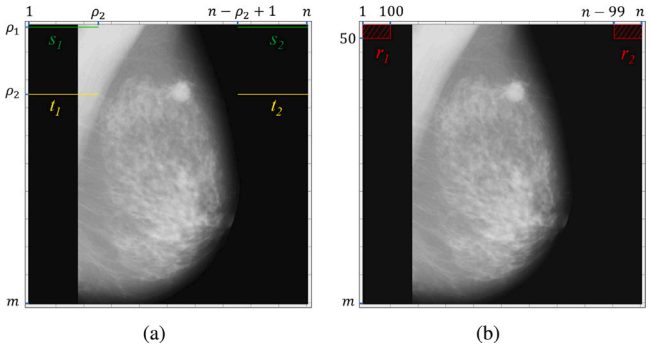

Fig. 3. An example of breast orientation discrimination in mammograms.

orientation discrimination method was developed by calculating pixel values in the upper-right and upper-left areas of a given mammogram. First, the row and column sizes were expressed as m and n, respectively, as shown in Fig. 3. All pixels in rows ρ_1 and ρ_2 of the image were then separately converted to arrays A_1 and A_2 based on the characteristics of the breast region at that position. The sum of elements from 1 to ρ_2 in A_1 were then calculated and expressed as s_1. The sum of elements from $(n-\rho_2+1)$ to n in A_1 is denoted s_2, the sum of elements from 1 to ρ_2 in A_2 is denoted t_1, and the sum of elements from $(n-\rho_2+1)$ to n in A_2 is denoted t_2. The sum of pixels in the region $[1:50, 1:100]$ is represented by r_1 and the sum of pixels in the region $[1:50, n-99:n]$ is represented by r_2. It is evident that $s_1 = s_2$ and $t_1 = t_2$ describe a breast region that may not have been detected. Therefore, ρ_2 must be gradually enlarged to recalculate the parameters t_1, t_2, s_1, and s_2. Finally, breast orientation in the mammogram can be inferred as follows:

$$F = \begin{cases} 1 & \text{if } r_2 > r_1 \parallel s_2 \geq s_1 \;\&\; t_2 > t_1 \\ 0 & Otherwise \end{cases}, \tag{4}$$

where F equal to 1 suggests a breast orientation to the left. Otherwise, the breast is assumed to be oriented to the right.

The proposed pectoral muscle removal technique can be represented as follows:

Step 1: Images of the breast oriented to the left are labeled and horizontally flipped to the right to quickly and precisely identify the location of the pectoral muscle. In other words, $(x_1, x_2, \ldots, x_{n-1}, x_n)$ is converted into $(x_n, x_{n-1}, \ldots, x_2, x_1)$, where x_i $(1 \leq i \leq n$ and n is the

Algorithm 1: Artifact removal in the breast region.

Input: A mammogram W and a mask image M
Output: An adjusted mask image W' and an adjusted mammogram M'

$[m,n] = size(M)$ //Calculate the row and column sizes of M
for $k = 1:1:n$ **do**
  //Calculate the pixel sum of each row in M
  $\mu(k) = sum(M(k, 1:n))$
$[Max, i] = max(\mu)$, $[Min, j] = min(\mu)$ //Max and Min are the maximum and minimum values in μ; i and j are their indices
if $Max - Min > 200$ & $W(i,10) - W(j,10) > 50$ **then**
  //Adjust W and M to remove the artifact
  $W' = W(i:m, 1:n)$, $M' = M(i:m, 1:n)$
for $k = 1:1:100$ **do**
  //Detect artifact
  if $\mu(k) > (n - n/3)$ **then**
    continue
  else
    break
for $r = k+1:1:100$ **do**
  if $\mu(k) - \mu(r) > 200$ **then**
    //Adjust W and M to remove the artifact
    $W' = W(r:m, 1:n)$, $M' = M(i:m, 1:n)$
if $\mu(i) - \mu(j) > 100$ & $i > j$ **then**
  //Adjust M to remove the artifact
  $M'(M[1:j, 1:i]) = 1$

column size of the image) represents all pixels in the ith column of the image.

Step 2: The sum of all pixels in each column was calculated and stored in an array B, used to identify the left meaningless rectangular background for the breast region (as shown in Fig. 3). If $B(i) \neq B(i+1)$ and $1 \leq i < n$, the left rectangular background (i.e., from the first to the ith column in the mammogram) is removed to reduce computational costs and facilitate localization of the rough pectoral muscle region.

Step 3: A local area in the upper-left of the mammogram image is automatically selected. The width (x) and height (y) of this area can be acquired explicitly as follows:

$$f(\xi) = \begin{cases} x = 100,\ y = \sigma/3 & \text{if } \xi < 100 \\ x = 150,\ y = \sigma/3 & \text{if } 100 \leq \xi < 150 \\ x = 200,\ y = \sigma/3 + 100 & \text{if } 150 \leq \xi < 250 \\ x = 300,\ y = \sigma/3 + 100 & \text{if } 250 \leq \xi \end{cases}, \tag{5}$$

where σ represents the maximum bound of the breast region in the vertical direction and ξ denotes the maximum bound of the pectoral muscle in the horizontal direction.

Step 4: The local area identified in Step 3 is employed to calculate a threshold value (θ) using the Otsu thresholding technique. A mask image of the mammogram can then be acquired using:

$$M = \sum_{i=1}^{m}\sum_{j=1}^{n} M_{ij} = \begin{cases} 1 & \text{if } \kappa_{ij} \geq \theta \\ 0 & Otherwise \end{cases}, \tag{6}$$

where M represents the mask image, m and n denote the row and column sizes of the mammogram, respectively, and κ_{ij} is a pixel in the mammogram. The area of each connected component in M is then used to identify and remove noise.

Step 5: An effective method for adhesive tape artifact detection is introduced to lessen the interference of this artifact during pectoral muscle removal. The artifact is first detected using Algorithm 1 and the mask image and mammogram are then modified to improve pectoral muscle removal.

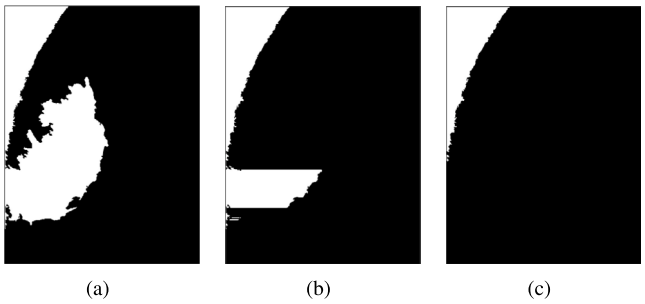

Fig. 4. The rough pectoral muscle region obtained using morphological operations. (a) A mask image of the rough pectoral muscle region connected with breast tissue, including the (b) semi-final and (c) final results for the mask image in the rough pectoral muscle region.

6	8	9	8	7	8
7	8	4	3	11	7
1	9	10	3	4	6
2	18	2	4	5	8
3	1	11	5	9	2
8	2	3	64	5	3

(a)

6	8	9	8	7	8
7	8	4	3	11	7
1	9	10	3	4	6
2	18	2	4	5	8
3	1	11	5	9	2
8	2	3	64	5	3

(b)

Fig. 5. The proposed region growing technique. (a) Pixels in an image to be segmented, where the initial seed point is shaded (the number 3). (b) The results of region growing with a maximum growth condition of 2.

Step 6: A rough pectoral muscle region is identified by detecting connected components in the upper-left region of the mask image. This region must then be processed further using morphological operations to separate the muscle from breast tissue. The specific steps involved can be described as follows:

(1) All pixel values in each row of the rough pectoral muscle mask image (χ) are stored in an array τ_i, where the row and column sizes of χ are respectively denoted by m and n, and $1 \leq i \leq m$. If $\tau_i(j) = 1$, j is stored in an array υ_1, where $1 \leq j \leq n$. The area from $\chi(i, \upsilon_1(k_1))$ to $\chi(i,n)$ is then removed by comparing $\upsilon_1(k_1)$ with $\upsilon_1(k_1 - 1)$, where $2 \leq k_1 \leq n_1$ and n_1 is the size of the υ_1.
(2) Further processing of the acquired results involves storing the sum of all pixels in each row of χ in an array υ_2. Likewise, the area from $\chi(k_2, \upsilon_2(k_2 - 1))$ to $\chi(k_2, n)$ is changed to black (zero) by comparing $\upsilon_2(k_2)$ with $\upsilon_2(k_2 - 1)$, where $2 \leq k_2 \leq m$.

An example of this process is illustrated in Fig. 4, where a rough pectoral muscle region was separated from breast tissue using the technique discussed above.

Step 7: The results obtained in Step 6 are further processed to refine the rough pectoral muscle region as follows:

(1) The height of χ is adjusted by comparing the area of the breast region with the area of χ. The hypotenuse can then be determined from the width and adjusted height of χ using the Pythagorean theorem, generating a mask image with a right triangle positioned in the upper-left region of the mask.
(2) If this triangle mask image contains the rough pectoral muscle mask image, the triangle mask is assumed to be the refined pectoral mask image. Otherwise, the triangle is re-calculated by enlarging the width and height of χ.

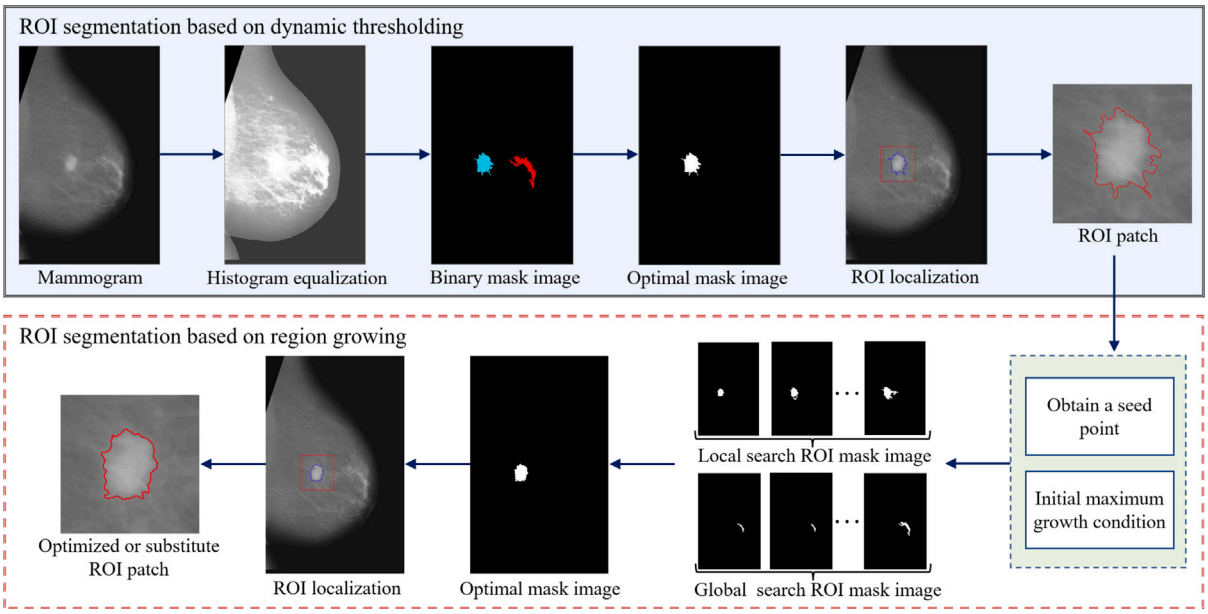

Fig. 6. A framework for the automated segmentation strategy using the dynamic thresholding and region growing algorithms.

Finally, the pectoral muscle region can be removed by replacing pixel values in the mammogram (which correspond to the refined pectoral muscle mask image) with pixel values from the background.

4. ROI segmentation based on dynamic thresholding and region growing

The ROI is of great importance as it is used by radiologists to detect breast cancer abnormalities. However, multiple ROIs may exist in mammograms simultaneously and identifying an optimal ROI can be a challenging task (i.e., the suspicious lesion). Generally, manual ROI segmentation requires a professional radiologist to mark the lesion, segmenting the mammogram in a highly inefficient and tedious process. In this section, an effective ROI segmentation strategy is proposed using the combined methods of dynamic thresholding and region growing, to automatically identify an optimal ROI for breast cancer detection. A framework for this segmentation strategy is shown in Fig. 6.

4.1. ROI segmentation based on dynamic thresholding

Thresholding is a simple, fast, and easily implemented segmentation algorithm that is widely applied to complex images (Wadhwa, Bhardwaj, & Singh Verma, 2019). An effective ROI segmentation strategy is proposed here, using dynamic thresholding, to improve the efficiency of breast cancer detection. The specific steps can be described as follows:

Step 1: Histogram equalization is applied to the mammogram to highlight multiple ROIs. Eq. (6) is then used to generate a mask for the mammogram, based on a given initial threshold (θ_1). In addition, noise in the mask image is removed by calculating the area of connected components in the mask, to reduce their effect on ROI segmentation.

Step 2: Algorithm 2 is used to identify an optimal ROI from the mask image obtained in Step 1, by first removing abnormal areas (such as the residual pectoral muscle in the bottom-left region of the MLO view). Furthermore, the circularity feature used in Algorithm 2 is defined as:

$$Circularity = \frac{4\pi \times A}{P^2}, \tag{7}$$

where A is the area of an ROI and P is the perimeter of the ROI.

Step 3: If the mask image acquired in Step 2 does not include a suspicious lesion, the initial threshold θ_1 can be dynamically adjusted with a given step length to reproduce the mask image until it includes the suspicious lesion.

Step 4: Connected components in the mask image are considered to be different ROI mask images. The area and circularity of each ROI mask is calculated and stored in the arrays α and β, respectively. In addition, the average intensity corresponding to each ROI in the mammogram is calculated and stored in the array γ. An optimal ROI mask image is

Algorithm 2: Abnormal area removal in ROIs.

Input: A mammogram W and a mask image M
Output: An adjusted mask image W' and an adjusted mammogram M'

$[m, n] = size(M)$ //Calculate the row and column sizes of M
$[labelImage, number] = labeled(M)$ //M is labeled
//Calculate the area, circularity, and major axis length of each connected component
for $i = 1 : number$ **do**
  $c_1(i) = Area(labelImage(i))$
  $c_2(i) = Circularity(labelImage(i))$ //using Eq. (7)
  $c_3(i) = MajorAxisLength(labelImage(i))$
//Remove residual pectoral muscle based on the position, area, and circularity of the connected component
for $i = 1 : 1 : m$ **do**
  for $j = 1 : 1 : n$ **do**
    if $W(i,1) = 10$ & $W(i,j) \neq 10$ & $M(i,j) > 1$ **then**
      $labelImage(labelImage == labelImage(i,j)) = 0$
    if $c_2 < 0.2 || (c_2 > 0.2$ & $c_1 < 2000)$ **then**
      $labelImage(labelImage == labelImage(i,j)) = 0$
    if $m/4 < i < m - m/4$ & $c_2 < 0.2 || (c_2 > 0.2$ & $c_1 < 2000)$ **then**
      $labelImage(labelImage == labelImage(i,j)) = 0$
    $d_1 = max(breast)$ //Calculate the maximum bound of the breast region in the vertical direction
    if $sum(M(d_1 - 100 : d_1, 1 : 100)) > 0$ **then**
      //Remove the abnormal areas $M(d_1 - 100 : d_1, 1 : 100) = 0$
//Remove the abnormal areas according to c_3
for i=1:number **do**
  if $c_3(i) > 200$ **then**
    $labelImage(labelImage == i) = 0$

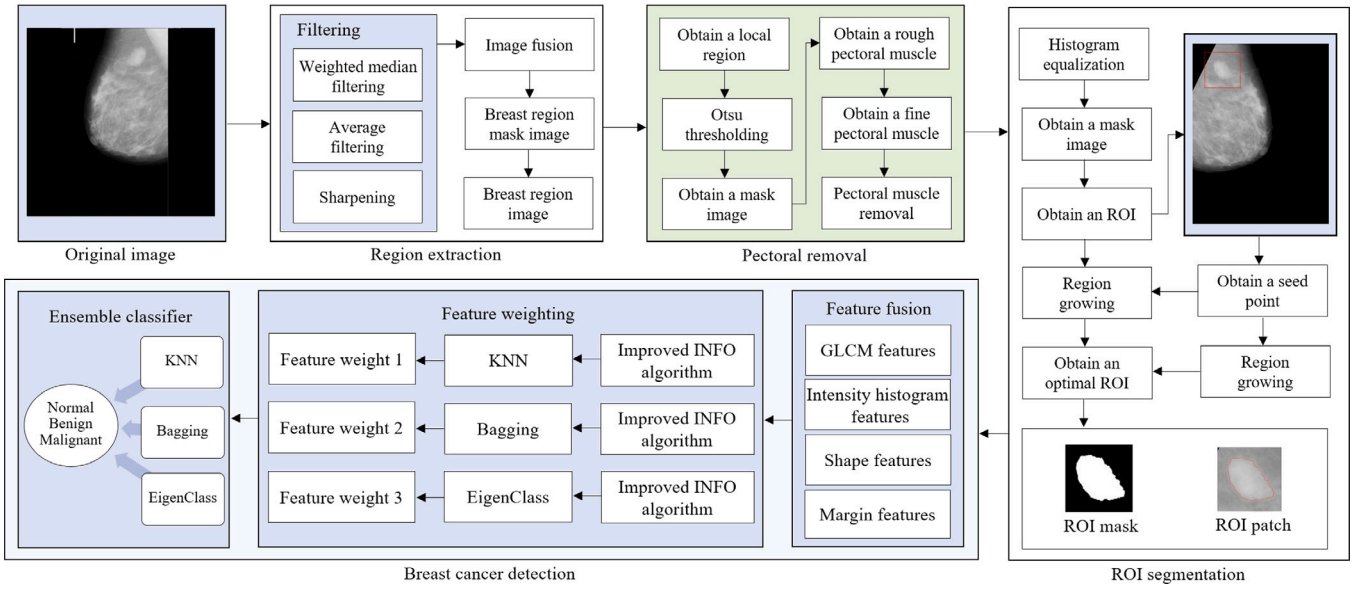

Fig. 7. A diagram of the proposed breast cancer detection strategy for CAD in mammograms.

then acquired from α, β, and γ as follows:

$$\ell_1 = \begin{cases} i & \text{if } |\gamma(i)-\gamma(j)|<5 \;\&\; |\beta(i)-\beta(j)|>0.1 \;\&\; \alpha(i)>1000 \\ j & Otherwise \end{cases}, \tag{8}$$

where i and j indicate the optimal ith and jth ROI mask images, determined by their circularity and average intensity.

Step 5: An ROI (i.e., suspicious lesion) in the mammogram can then be localized using the optimal ROI mask image acquired in Step 4. The ROI patch can simultaneously be acquired and used to calculate textural features for breast cancer detection.

ROI patch localization in a mammogram can be achieved using the technique discussed above. If average pixel values in the suspicious lesion are lower than those of the breast tissue, or if the given threshold is too large, the suspicious lesion is likely to go undetected as the ROI boundary may be obscured. This boundary is an important feature used to distinguish between benign and malignant masses and it is therefore necessary to further optimize the algorithm to achieve a more accurate ROI.

4.2. Optimized ROI segmentation based on region growing

Region growing is an effective segmentation technique that is widely used to segment ROIs in medical images (Rodrigues, Conci, & Liatsis, 2020). This process involves detecting neighboring pixels in an initial seed point and determining whether to add these pixels to a given region using a maximum growth condition, as illustrated in Fig. 5. An optimized ROI segmentation algorithm, based on region growing, is proposed in this study. In this process, average pixel values in an ROI are calculated and considered to be seed points for region growing, expanding the ROI image using a maximum growth condition. These seed points can also be used to search for more accurate ROIs in the mammogram, substituting selected ROIs as discussed in Section 4.1. The specific steps in this segmentation process can be described as follows:

Step 1: Various thresholds are initialized and considered to be growth conditions for the region growing technique. Seed points (i.e., average pixel values in the ROI) are then used to grow the ROI patch, based on different maximum growth conditions, producing several ROI mask images. Abnormal areas in the masks are then removed using Algorithm 2.

Step 2: The area and circularity of each connected component in the mask images acquired in Step 1 are calculated and stored in the arrays p_1 and p_2, respectively. The circularity of the current selected ROI mask image is also calculated and expressed as p. An optimal ROI mask image, selected from p_1, p_2, and p, can then be expressed as:

$$\ell_2 = \begin{cases} i & \text{if } p_2(i)-p > 0.1 \\ j & \text{if } p_2(i)-p_2(j)<0.05 \;\&\; p_1(j) > p_1(i) \\ k & \text{if } p_2(j)-p_2(k)<0.05 \;\&\; p_1(k) > p_1(j) \end{cases}, \tag{9}$$

where i, j, and k indicate the ith, jth, and kth connected components in the optimal ROI mask image. This calculation is performed using circularity values, where $p_2(i) > p_2(j) > p_2(k)$. The ℓ_2 ROI mask image exhibits clearer boundary information than the ROI mask acquired in Section 4.1.

Step 3: The seed point obtained in Step 1 grows in the mammogram to produce various mask images using the initial maximum growth condition, which are then stored in an array K. The abnormal regions in K are then removed using Algorithm 2. The circularity and average intensity of each ROI mask image in K is then calculated and saved to the arrays α_i and β_i, respectively, as part of a global search for an ROI substitute in the mammogram. This condition can be represented as:

$$\ell_3 = \begin{cases} j & \text{if } \alpha_i(j)-\kappa>0.1 \;\&\; \alpha_i(j)>0.4 \;\&\; \beta_i(j)>160 \\ 0 & Otherwise \end{cases}, \tag{10}$$

where j is a connected component denoting an optimal ROI in α_i and κ is a circularity feature in the current optimal ROI. If ℓ_3 is equal to 0, this indicates that no ROI substitute is available. Otherwise, ℓ_3 represents an ROI in the ith mask image (i.e., $K(i)$) and is considered an optimal ROI.

Step 4: The ℓ_3 ROI in $K(i)$ is optimized using the method described in Step 2 if a substitute ROI exists in the mammogram. The characteristics of nipples in mammograms are similar to those of masses. As such, it is necessary to determine whether an ROI is a nipple using its area, circularity, and position, for substitution in the previous ROI. Subsequently, ROI patches and localization in mammograms can be achieved using the optimal ROI mask image.

Finally, an ROI superior to that of Section 4.1, with clear boundary features and more exactness, can be obtained using the method described above. The textural and morphological features of the acquired ROI can then be extracted and considered to be the input to an ensemble classifier.

Table 1
A description of features in the proposed technique.

No.	GLCM Features (Nabizadeh & Kubat, 2015)	Intensity Histogram Features (Nabizadeh & Kubat, 2015)	Margin Features (Joo, Yang, Moon, & Kim, 2004; Kilday, Palmieri, & Fox, 1993)	Shape Features (Joo et al., 2004; Kilday et al., 1993; Rouhi & Jafari, 2016)
1	Energy	Mean	Spiculation	Area
2	Correlation	Variance	Eccentricity	Major Axis Length
3	Inverse Difference	Skewness	Roundness	Minor Axis Length
4	Homogeneity	Kurtosis	Circularity	Convex Area
5	Contrast	Energy	Ellipsoid	Diameter
6	Entropy	Entropy	Roughness	Solidity
7	Absolute Value	Null	Branch Pattern	Perimeter
8	Maximum Probability	Null	Null	Extent
9	Null	Null	Null	Orientation
10	Null	Null	Null	Mean Intensity
11	Null	Null	Null	Brightness
12	Null	Null	Null	Acreage Ratio
13	Null	Null	Null	NRL[a] Mean
14	Null	Null	Null	NRL Standard Deviation
15	Null	Null	Null	Radial Length Histogram Entropy

[a]NRL: Normalized Radial Length.

5. Breast cancer detection based on an ensemble classifier and feature weighting

Early detection of breast cancer is of great significance as it provides timely treatment and prolongs patient life expectancy. Machine learning algorithms are powerful and effective techniques that are widely applied for breast cancer diagnosis using CAD systems (Yassin et al., 2018). Specifically, EigenClass, a recently proposed machine learning algorithm, has achieved promising performance for classification problems (Erkan, 2021). In order to further improve classification results for breast cancer detection using mammogram images, an ensemble classifier model is proposed by combining typical KNN and bagging algorithms with a new EigenClass model. Each feature in the dataset exerts varying influence on the classification results and feature weighting can be used to assign weights to each feature, according to its importance for classification. Therefore, an improved INFO algorithm is proposed using an opposition-based learning method, which is then developed as a feature weighting technique to further improve detection accuracy. The resulting ensemble classifier model can preferably categorize suspicious lesions as normal, benign, or malignant tumors using a majority voting rule.

5.1. Feature weighting based on an improved INFO algorithm

INFO is a novel optimization algorithm based on the weighted mean of vectors, offering superior capabilities for solving complex engineering problems (Ahmadianfar, Heidari, Noshadian, Chen, & Gandomi, 2022). An improved INFO algorithm with accelerated convergence is proposed in this study, using an opposition-based learning method. Feature weighting is also included to improve the accuracy of breast cancer diagnosis. The impact of feature weights on mammogram classification was evaluated using an objective function defined as:

$$\Gamma(\varphi) = 1 - \frac{\alpha_1 + \alpha_2}{\alpha_1 + \alpha_2 + \beta_1 + \beta_2}, \tag{11}$$

where φ is the weight of features extracted from the ROI (i.e., a solution of the objective function) and α_1, α_2, β_1, and β_2 respectively denote true positive, true negative, false positive, and false negative results in a mammogram diagnosis. In this calculation, smaller objective function values represent better assigned feature weights for mammogram classification. The specific feature weighting algorithm can be described as follows:

Step 1: All parameters in the INFO algorithm are initialized, including the population size (N), the current and maximum iterations ($g, MaxIter1,$ and $MaxIter2$), the upper and lower boundaries of the variables (ub and lb), and the population dimension (dim). Note the number of features extracted from the ROI in the mammogram is equal to dim.

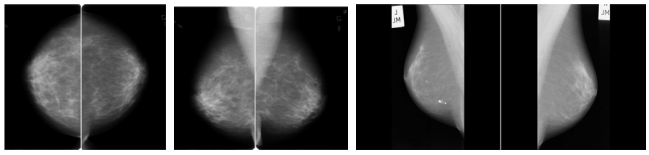

(a) (b) (c)

Fig. 8. Various mammogram views. (a) The CC view in the DDSM dataset; (b) the MLO view in the DDSM dataset; (c) the MLO view in the MIAS dataset.

Step 2: Variables in the population are initialized and represented as:

$$x = \rho_1 \times (ub - lb) + lb, \tag{12}$$

where ρ_1 is a random number satisfying $0 < \rho_1 < 1$. Furthermore, all initialized variables can be expressed as $X_i = \{x_1^i, x_2^i, \ldots, x_{dim-1}^i, x_{dim}^i\}$, where $1 \le i \le N$. Here, X_i represents a solution to the objective function.

Step 3: A new variable in the population can be obtained using opposition-based learning (Gupta, Deep, Heidari, Moayedi, & Wang, 2020), to accelerate convergence of the INFO algorithm, represented by:

$$y = ub + lb - x, \tag{13}$$

where x represents an initialized variable in the population. All new variables can then be expressed as $Y_i = \{y_1^i, y_2^i, \ldots, y_{dim-1}^i, y_{dim}^i\}$.

Step 4: The variables in X_i and Y_i are used to construct a new population denoted by $Z_j = \{z_1^j, z_2^j, \ldots, z_{dim-1}^j, z_{dim}^j\}$, where $1 \le j \le 2N$. If $z_l^j < 0.5$, the weight of the lth feature extracted from the ROI is set to 0; otherwise it is set 1, where $1 \le l \le dim$. All feature weights can be assigned according to Z_j and used to calculate the objective function value given by Eq. (11), which is saved to the array $Cost$ (i.e., $Cost = \{\Gamma(Z_1), \Gamma(Z_2), \ldots, \Gamma(Z_{j-1}), \Gamma(Z_j)\}$). The updated initial variables can then be acquired by selecting solutions for the first N elements after sorting $Cost$ in descending order (i.e., $Z_k = \{z_1^k, z_2^k, \ldots, z_{dim-1}^k, z_{dim}^k\}$), where $1 \le k \le N$.

Step 5: The solutions $Cost(1)$ and $Cost(N)$, obtained from the sorted $Cost$ array in Step 4, can be considered the best and worst solutions and are expressed as Z_{bs} and Z_{ws}, respectively. A random number (ι) is also generated, where $\iota \in \{2, 3, 4, 5\}$. The solution of $Cost(\iota)$ is considered to

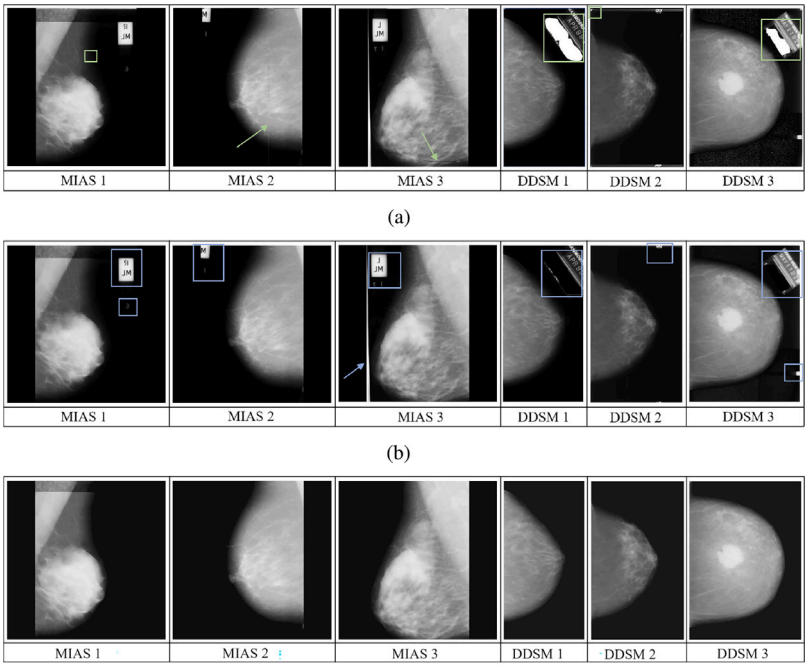

Fig. 9. The proposed breast region extraction technique. (a) The original image; (b) noise removal and image enhancement; (c) the breast region extracted from (a).

be a better solution and is denoted Z_{bt}. Each solution in Z_k is then updated in turn using the following steps applied to Z_{bs}, Z_{ws}, and Z_{bt}.

Step 6: An update rule operator in the INFO algorithm is used to increase the population's diversity. This rule can be used to generate two new vectors given by:

$$z1 = \begin{cases} Z_k + \sigma \times \zeta + \rho_1 \times \frac{Z_{bs} - Z_{a1}}{\Gamma(Z_{bs}) - \Gamma(Z_{a1}) + 1} & \text{if } \rho_2 < 0.5 \\ Z_{a1} + \sigma \times \zeta + \rho_1 \times \frac{Z_{a2} - Z_{a3}}{\Gamma(Z_{a2}) - \Gamma(Z_{a3}) + 1} & Otherwise \end{cases}, \tag{14}$$

$$z2 = \begin{cases} Z_{bs} + \sigma \times \zeta + \rho_1 \times \frac{Z_{a1} - Z_{a2}}{\Gamma(Z_{a1}) - \Gamma(Z_{a2}) + 1} & \text{if } \rho_2 < 0.5 \\ Z_{bt} + \sigma \times \zeta + \rho_1 \times \frac{Z_{a1} - Z_{a2}}{\Gamma(z_{a1}) - \Gamma(Z_{a2}) + 1} & Otherwise \end{cases}, \tag{15}$$

where ζ is a vector generated from Z_{bs}, Z_{bt}, and Z_{ws}, ρ_1 is a normally distributed random number, ρ_2 is a randomly generated number ($0 < \rho_2 < 1$), $a_1, a_2, a_3 \in \{1, 2, \ldots, N-1, N\}$, $a_1 \neq a_2 \neq a_3 \neq k$, and σ is a scaling rate for the vector, defined as:

$$\sigma = \left[2 \times exp\left(\frac{-4 \times g}{IterMax}\right)\right] \times (2 \times \rho_2 - 1), \tag{16}$$

where ρ_2 denotes a randomly generated number ($0 < \rho_2 < 1$).

Step 7: A new solution is generated by combining $z1$ and $z2$ to improve the algorithm's local search capabilities, which can be expressed as:

$$\mu_1 = \begin{cases} z1 + (0.05 \times \rho_1) \times |z1 - z2| & \text{if } \rho_2 < 0.5 \\ z2 + (0.05 \times \rho_1) \times |z1 - z2| & Otherwise \end{cases}, \tag{17}$$

where ρ_1 and ρ_2 are randomly generated numbers and $0 < \rho_1, \rho_2 < 1$. If $g < MaxIter1$, features extracted from the mammogram are assigned weights using the variables in μ_1 as follows:

$$y_i = \begin{cases} 0 & \text{if } x_i < 0.5 \\ 1 & Otherwise \end{cases}, \tag{18}$$

where x_i indicates the ith variable in μ_1 and y_i represents the assigned weight of the ith feature. Otherwise, the variables in μ_1 represent the weights of the features. The objective function value for μ_1 is denoted $\Gamma(\mu_1)$. If $\Gamma(\mu_1) < Cost(k)$, the $Cost(k)$ is replaced with $\Gamma(\mu_1)$ and Z_k is replaced with μ_1 to update the current solution and its objective function.

Step 8: Another new solution is randomly generated to prevent the algorithm from dropping into locally optimal solutions, thereby promoting the exploration of global optima. A new solution based on a random number defined between 0 and 1 can be formalized as:

$$\mu_2 = \begin{cases} Z_{bs} + \alpha \times [\zeta + \alpha \times (Z_{bs} - Z_{a1})] & \text{if } \rho_2 < 0.5 \\ Z_r + \alpha \times [\zeta + \alpha \times (v_1 \times Z_{bs} - v_2 - z_r)] & Otherwise \end{cases}, \tag{19}$$

where α is a random number with a normal distribution, ρ_2 denotes a randomly generated number ($0 < \rho_2 < 1$), v_1 and v_2 are respectively random numbers used to increase the impact of the best position on a vector. The term Z_r denotes a vector given by:

$$Z_r = \rho_2 \times Z_{avg} + (1 - \rho_2) \times [\rho_2 \times Z_{bs} + (1 - \rho_2) \times Z_{bs}], \tag{20}$$

where ρ_2 is a randomly generated number ($0 < \rho_2 < 1$), Z_{avg} is equal to $(Z_a + Z_b + Z_c)/3$. Likewise, if $g < MaxIter1$, the features are assigned weights according to the variables in μ_2, defined by Eq. (18). Otherwise, the variables in μ_2 are used to represent the feature weights. The objective function value for μ_2 is then calculated and denoted $\Gamma(\mu_2)$, for comparison with the objective function of the current solution. Specifically, if $\Gamma(\mu_2) < Cost(k)$, $Cost(k)$ is replaced by $\Gamma(\mu_2)$ and Z_k is replaced by μ_2.

Step 9: The *Cost* array is sorted in descending order once all solutions in the population are updated. If $g < MaxIter2$, the algorithm is iterated to identify an optimal solution by updating Z_{bs}, Z_{bt}, and Z_{ws} in Step 5. The optimal weights of features extracted from the mammogram (i.e., Z_{bs}) can then be acquired using the improved INFO algorithm.

Finally, each of the features extracted from the mammogram ROI can be assigned an optimal weight using a feature weighting algorithm, to further improve classification performance. It is worth noting the redundant and unimportant features can be removed by assigning feature weights to 0.

5.2. Breast cancer detection with an ensemble classifier model

In this section, an ensemble classifier model is designed using KNN, bagging, and EigenClass algorithms and applied to assist radiologists

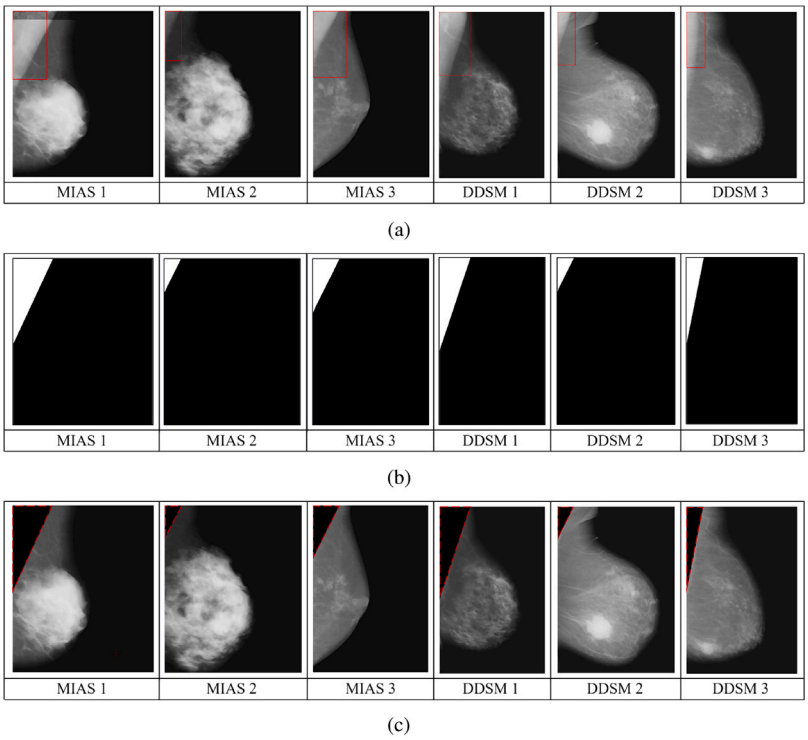

Fig. 10. The proposed pectoral muscle removal process. (a) The flipped image. (b) Mask images of the refined pectoral muscle region. (c) The results of pectoral muscle removal.

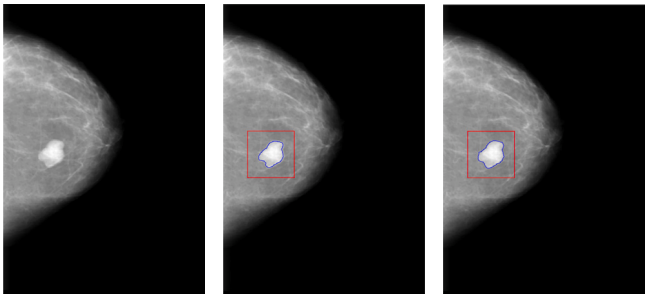

Fig. 11. ROI segmentation of a DDSM mammogram. (a) The original image; (b) the localized ROI; (c) the optimized ROI.

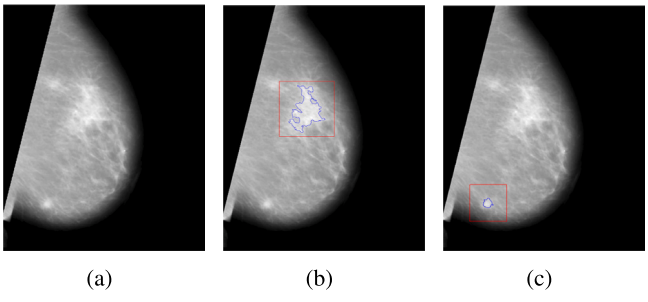

Fig. 12. ROI segmentation of an MIAS mammogram. (a) The original image; (b) the localized ROI; (c) the substitute ROI.

in detecting breast cancer in mammograms. A schematic diagram of the proposed breast cancer detection strategy is shown in Fig. 7. In this process, region extraction and pectoral muscle removal are first accomplished, as described in Section 3. Textural and morphological features are then extracted from the segmented ROI using the steps formulated in Section 4, to construct a new feature vector. These weighted features are considered a basis for breast cancer detection, using an ensemble classifier model with a majority voting rule to determine whether a mammogram exhibits a normal, benign, or malignant tumor. A detailed summary of the proposed strategy, after ROI segmentation, is provided below:

Step 1: Features extracted from the ROI can be divided into textural and morphological samples. Textural features include gray-level co-occurrence matrix (GLCM) and intensity histogram features, while morphological features include shape and margin features. In this study, a total of 44 features were extracted from the ROI (as shown in Table 1) and used to produce a new feature vector for breast cancer detection.

Step 2: Data in each feature were normalized using a Max-Min method (Pollesch & Dale, 2016) to accelerate model convergence and reduce the influence of abnormal data on the classifier. As described in the feature weighting algorithm proposed in Section 4.1, the weight of each feature extracted from the ROI is used to further improve classification accuracy. In this process, KNN, bagging, and EigenClass are implemented to obtain optimal feature weights for each classifier used as inputs to the ensemble classifier model.

Step 3: The ensemble classifier model is constructed by combining the KNN, bagging, and EigenClass classifiers, where the bagging classifier includes ten decision trees to reduce variance and prevent overfitting. Breast cancer detection in mammograms is implemented using weighted features based on these three classifiers. The training dataset was first used to train the classifier, which was then provided with test data that were categorized as normal, benign, or malignant tumors. Finally, results for the ensemble classifier model were obtained by a majority voting rule, calculated using a 3:4:3 ratio for the prediction results from KNN, bagging, and Eigenclass classifiers.

Finally, breast cancer detection was achieved in mammograms using the techniques discussed above, to assist radiologists in diagnosis. Noise and trivial objects in the images were removed to constrain the search region for suspicious breast lesions. Pectoral muscles were also removed

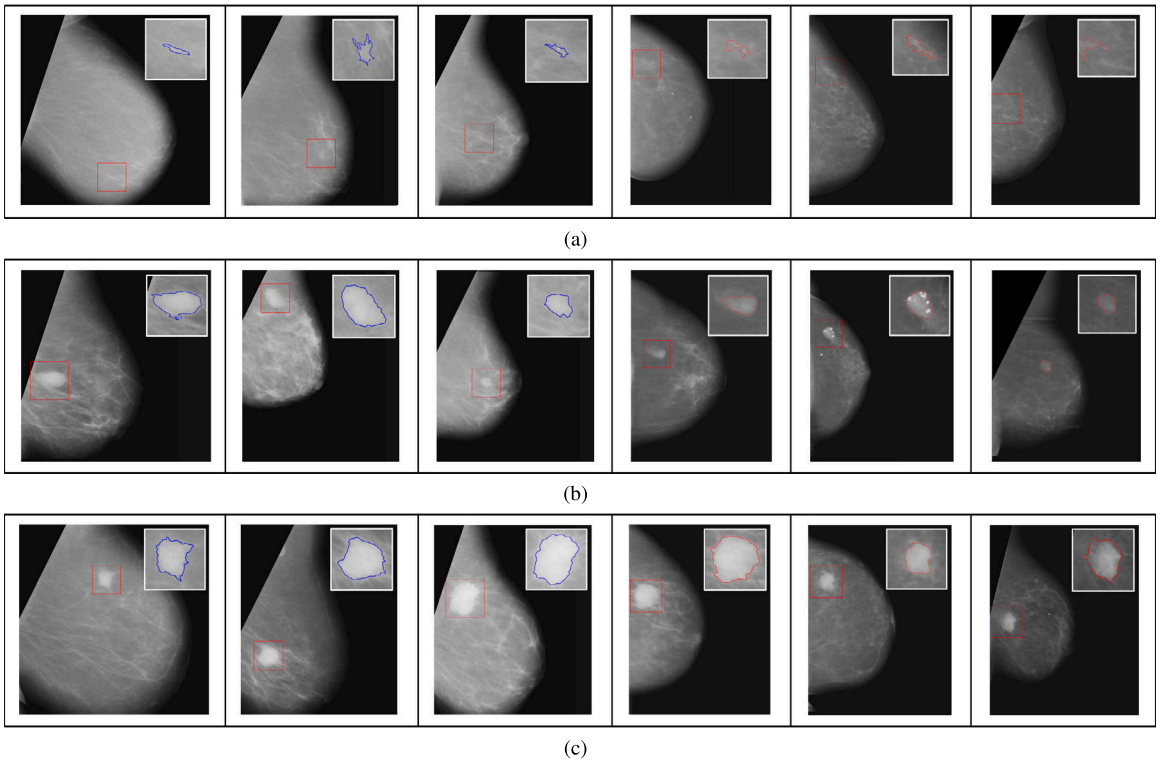

Fig. 13. ROI segmentation in (a) normal, (b) benign, and (c) malignant mammograms.

Table 2
Initial INFO algorithm parameters.

N	*dim*	*g*	*lb*	*ub*	*MaxIter1*	*MaxIter2*
100	44	1	0	1	200	500

Table 3
Breast cancer detection results for the proposed scheme applied to the MIAS dataset.

Split data	MIAS dataset				
	Acc (%)	Pre (%)	Rec (%)	F-1 (%)	Spe (%)
1-Fold	93.33	86.81	72.22	90.00	91.37
2-Fold	96.67	97.92	88.89	95.00	93.33
3-Fold	96.67	97.92	91.67	95.00	93.33
4-Fold	90.00	91.67	55.56	85.00	80.00
5-Fold	86.67	89.47	50.00	80.00	73.33
6-Fold	93.33	84.38	66.67	90.00	91.37
7-Fold	90.00	94.44	61.11	85.00	80.00
8-Fold	86.67	89.47	50.00	80.00	73.33
9-Fold	86.67	89.47	50.00	80.00	73.33
10-Fold	90.00	94.44	61.11	85.00	80.00
Average	91.00	91.60	64.72	86.50	82.94

to reduce interference. A segmentation strategy was then formulated, based on dynamic thresholding and region growing, to automatically segment, select, and locate ROIs. Extracted and weighted features from the ROI were used to predict breast cancer by applying the proposed ensemble classifier model.

6. Experimental settings and result analysis

A series of experiments were conducted to verify the effectiveness of the proposed breast cancer detection technique. The DDSM and MIAS datasets were used in these experiments to evaluate the performance of the proposed scheme. In this process, some commonly used evaluation metrics were adopted to measure the classification results. The advantages of the proposed model were assessed through a comparison with representative works conducted in recent years.

6.1. Datasets and evaluation metrics

The DDSM dataset was collected at the University of South Florida (Heath et al., 1998), where each case included four CC and MLO views for right and left breasts, as shown in Fig. 8(a) and (b). The DDSM set includes 12-bit and 16-bit grayscale images, with an average size of 3000×5000 pixels. Mammograms in MIAS are 8-bit grayscale images of size 1024×1024 pixels (Suckling, 1994), as shown in Fig. 8(c). The type of abnormality (benign or malignant) in these datasets can be classified as either calcification, well-defined, spiculated, architectural distortion, asymmetry, or ill-defined. In the experiment, 200 and 732 mammograms were randomly selected from the MIAS and DDSM datasets, respectively, excluding the calcification, architectural distortion, asymmetry, and density beast images, to objectively evaluate the proposed scheme. A 10-fold cross-validation (CV) technique was used to divide the data into training and test sets to obtain stable and reliable classification results. Specifically, the dataset was randomly split into ten smaller disjoint datasets of approximately equal size. Nine smaller datasets were selected as training data and the remaining set served as the test data.

Evaluation metrics used to measure the classification results included accuracy, precision, recall, F-measure, and specificity (Nanglia, Ahmad, Khan, & Jhanjhi, 2022), where F-measure combines both precision and recall into a single value that captures both properties. DDSM images were automatically adjusted using the '*imresize*' function to reduce computational costs (Yan, Huang, & Yu, 2022). This process can be represented as: $imresize(image, [m/\kappa, n/\kappa])$, where $image$ represents an image needing to be adjusted, m and n respectively denote the row and column sizes of the mammogram image, and $\kappa = round(m/1024)$.

Table 4
Breast cancer detection results for the proposed scheme applied to the DDSM dataset.

Split data	DDSM dataset				
	Acc (%)	Pre (%)	Rec (%)	F-1 (%)	Spe (%)
1-Fold	94.52	94.77	83.09	91.78	93.83
2-Fold	94.52	91.75	86.92	91.78	94.40
3-Fold	90.99	85.27	78.77	86.49	91.63
4-Fold	94.52	89.73	83.09	91.78	94.89
5-Fold	91.78	86.21	77.83	87.67	92.06
6-Fold	92.69	93.25	80.86	89.04	91.60
7-Fold	90.87	90.60	76.08	86.30	89.88
8-Fold	96.40	93.37	90.43	94.59	96.64
9-Fold	92.69	91.26	79.59	89.04	92.59
10-Fold	93.61	87.75	86.44	90.41	94.44
Average	93.26	90.40	82.31	89.89	93.20

6.2. Region extraction and pectoral muscle removal

The backgrounds of mammograms often contain noise and insignificant objects that can negatively influence the search for suspicious lesions. Therefore, the region extraction technique proposed in Section 3.1 was used to isolate breast ROIs from mammograms in the MIAS and DDSM datasets. The original images are shown in Fig. 9(a), where the green arrows and rectangular boxes provide supplemental annotations to emphasize digital, high-intensity, and straight-line noise. There is evidently a discrepancy in the lighting, exposure level, and background between images in Fig. 9(a). Digital and straight-line noise in these images was removed using different filtering techniques that enhanced contrast in the image. High-intensity noise was removed by identifying pixel values in the image that were greater than 250. Fig. 9(b) shows the image from Fig. 9(a) with the noise removed. The quality of images was simultaneously enhanced to a large extent. Multiple insignificant objects including scanning artifacts, orientation tags, and low-intensity labels (i.e., the annotations labeled by the blue arrows and rectangular boxes in Fig. 9(b)) were also present and required removal by extracting the breast region using the image fusion method developed in Section 3.1. The breast region shown in Fig. 9(c) was identified and extracted from Fig. 9(b), in which it is evident that all insignificant objects were removed using the proposed method. In addition, extracted regions not only exhibited breast contour information from the original image, but also high-fidelity detail without noise. Therefore, the proposed region extraction method not only removed noise from the mammograms, it also enhanced the quality of mammograms by reducing discrepancies in lighting and exposure levels, thereby constraining the search region for suspicious lesions.

Pixel intensity in the pectoral muscle is very similar to that of suspicious breast lesions, which makes it difficult to automatically and exactly locate ROIs in mammograms. Interference from the pectoral muscle was avoided during the identification of the ROI by removing the muscle from the breast region in MLO views of the mammogram, using the technique proposed in Section 3.2. The results of pectoral muscle removal are shown in Fig. 10, where images of the breast oriented to the left were horizontally flipped for fast localization of pectoral muscle position, as shown in Fig. 10(a). Note the left black background of the breast region in the images was entirely removed and the areas within the red rectangular boxes were automatically selected as local areas based on pectoral muscle characteristics. These regions were then used to generate a threshold value in the Otsu thresholding algorithm, for the purpose of acquiring a mask image of the mammogram. The resulting mask image of the refined pectoral muscle region, obtained by morphological operations, is shown in Fig. 10(b). Note the white areas in the mask image denote the pectoral muscle that will be removed from mammogram images in Fig. 10(a). To be specific, the pectoral muscle in the breast region was removed using the mask image of the refined region shown in Fig. 10(b), the results of which are shown in Fig. 10(c). Evidently, the high-intensity pectoral muscle in the images in Fig. 10(b) was all removed successfully. This demonstrates the proposed technique can effectively remove pectoral muscles from the breast region for reduced interference during ROI segmentation.

6.3. ROI segmentation and localization in mammograms

As previously mentioned, manual ROI segmentation is highly time-consuming. ROIs in CC and MLO mammogram views, with pectoral muscles removed, were automatically segmented and localized to improve the overall efficiency using the strategy formulated in Section 4. An optimal ROI was then selected, as shown in Figs. 11 and 12. In this process, an ROI is first identified using a dynamic thresholding method, as shown in Figs. 11(b) and 12(b). Here the red box is an annotation used to localize the ROI, the boundary of which is depicted in blue. Evidently, the boundary information of the ROI in Fig. 11(b) is not very clear. Therefore, the ROI was then optimized using a region growing method to provide clearer boundary information, so as to better distinguish between benign and malignant masses. The result of this process is shown in Fig. 11(c). A region growing method was also employed to globally search for a substitute and a better ROI in the mammogram, the results of which are shown in Fig. 12(c). Compared with the ROI in Fig. 12(b), the localized ROI in Fig. 12(c) is more likely to be a suspicious lesion.

The segmented and localized ROI results acquired from normal, benign, and malignant mammograms, shown in Fig. 13, verify the effectiveness of the proposed segmentation strategy. Note the red rectangular box in Fig. 13 includes annotations to emphasize the location of the ROI, as the segmented ROI patch is enlarged and shown in the upper-right region of the image. Normal, benign, and malignant mammogram cases are shown in Figs. 13(a), 13(b), and 13(c), respectively. ROI boundaries were delineated using blue and red to denote irregularities in MIAS and DDSM, respectively. The proposed ROI segmentation strategy not only located ROIs, it also clearly described the boundaries of benign and malignant tumors, verifying its effectiveness for automated ROI identification. ROIs segmented in mammogram images could be used to extract features for breast cancer detection.

6.4. Analysis of the proposed breast cancer detection strategy

The classification performance of the proposed breast cancer detection strategy, based on ensemble classifier and feature weighting algorithms, was evaluated experimentally to determine the resulting diagnostic accuracy. Textural and morphological features in the segmented ROIs were first extracted and fused to construct a new feature vector for input to the classifier. In addition, a 10-fold CV technique was adopted to divide the MIAS and DDSM data into training and test sets, respectively, with the aim of producing reliable classification results. Optimal weights for each feature in the vector were then assigned using feature weighting based on the improved INFO algorithm proposed in Section 5.1. A series of comparison experiments using the KNN, bagging, and EigenClass classifiers (applied to MIAS and DDSM data) were conducted to demonstrate the improved INFO algorithm outperformed the original INFO algorithm in searching for optimal solutions and the assignment of optimal weights. Initial parameters for the improved and original INFO algorithms are provided in Table 2. These algorithms were iterated 500 times and the results, compared using objective function values calculated by assigned feature weights, are shown in Fig. 14. Smaller objective function values indicate better assigned feature weights. It is evident the objective function values produced by the improved INFO algorithm are lower than those obtained by the INFO algorithm, notably in Fig. 14(a), (d), and (e). These results confirm the improved INFO algorithm can identify optimal solutions and assign optimal weights for each feature extracted from an ROI.

After obtaining the optimal feature weight by the improved INFO algorithm, the weighted features corresponding to the training data are used to train the KNN, bagging, and EigenClass classifiers. The trained

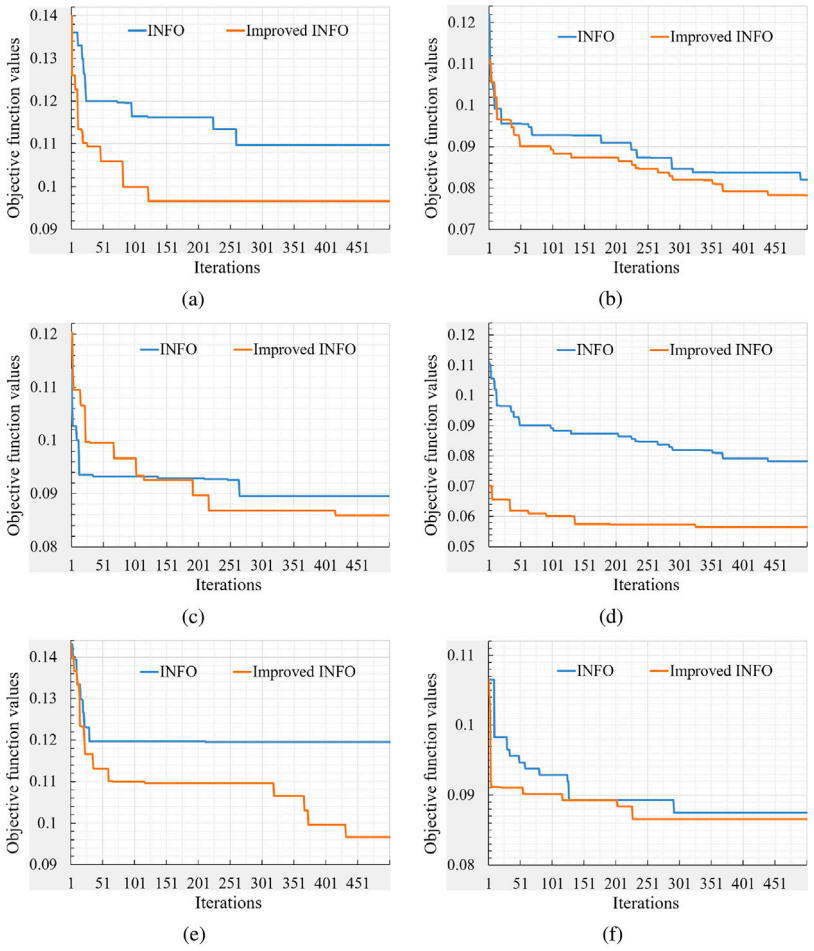

Fig. 14. Results produced by the INFO and improved INFO algorithms in the assignment of optimal feature weights. (a)–(b), (c)–(d), and (e)–(f) compare the results for objective function values calculated on the basis of weights assigned using KNN, bagging, and EigenClass classifiers in MIAS and DDSM data, respectively.

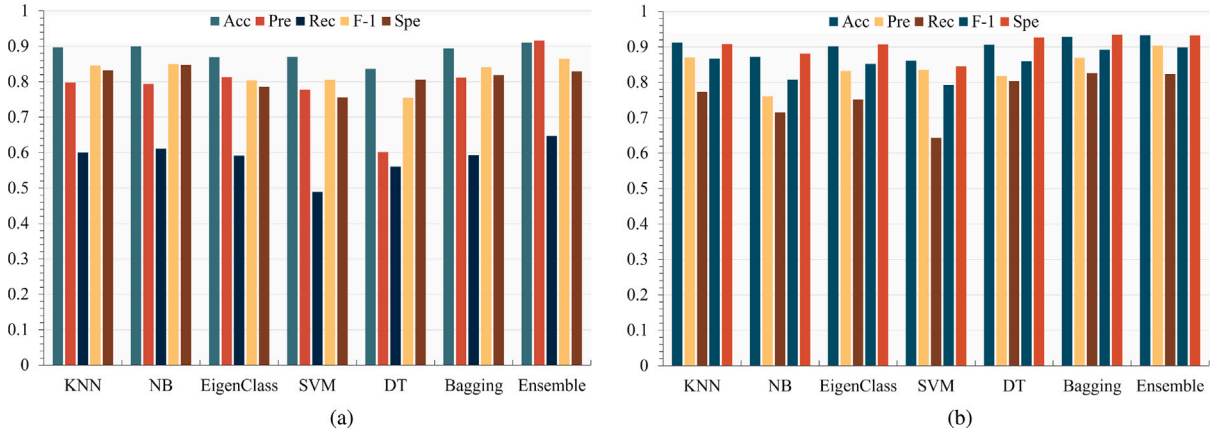

Fig. 15. A comparison of different classifiers used for breast cancer detection in the (a) MIAS and (b) DDSM datasets.

KNN, bagging, and EigenClass classifiers were respectively used to classify test data as normal, benign, or malignant tumors. Breast cancer classification results were then obtained using the ensemble classifier model and a majority voting rule. Predicted results for the MIAS data are provided in Table 3, where the average classification accuracy is seen to be 91.00% and the highest accuracy (96.67%) was achieved for 2-fold and 3-fold processes. Predicted results for the DDSM data are provided in Table 4, where the average classification accuracy is seen to be 93.26% and the highest accuracy (96.40%) was achieved for an 8-fold process. Additional evaluation metrics (i.e., accuracy (Acc), precision (Pre), recall (Rec), F-measure (F-1), and specificity (Spe)) are also provided for the two datasets. These experimental results demonstrate the proposed ensemble classifier model offers good performance for breast cancer classification. Therefore, the breast cancer detection strategy proposed in this paper, utilizing mammogram images, is highly practical and effective.

To further illustrate the advantages of this approach, various classifier models including SVM, Decision Tree (DT), KNN, EigenClass, bagging, and NB were employed for comparison with the proposed ensemble classifier. Similarly, a 10-fold CV was also used to calculate

Table 5
A comparison of the proposed scheme and related works applied to the MIAS dataset.

No.	Reference	Dataset	Predicted class	Validation	Classifier	Accuracy (%)
1	Milosevic, Jankovic, and Peulic (2015)	MIAS	Normal–Abnormal	5-Fold CV	SVM	62.00
					KNN	60.70
					NB	55.30
2	Dhahbi, Barhoumi, and Zagrouba (2015)	MIAS	Benign–Malignant	Leave-One-Out CV	KNN	81.35
3	Rouhi and Jafari (2016)	MIAS	Benign–Malignant	10-Fold CV	MLP[a]	87.71
4	Li, Ge, Zhao, Guan, and Yan (2018)	MIAS	Benign–Malignant	80–20%	CNN	89.05
5	Ting, Tan, and Sim (2019)	MIAS	Normal–Benign–Malignant	–	CNN	90.50
6	Shivhare and Saxena (2021)	MIAS	Benign–Malignant	–	NN[b]	84.85
7	Shaikh, Krishnan, and Thanki (2021)	MIAS	Normal–Abnormal	70–15–15%	CNN	87.5
8	Alruwaili and Gouda (2022)	MIAS	Benign–Malignant	80–20%	MOD-RES	89.5
					Nasnet-Mobile	70.00
9	Qasem et al. (2022)	MIAS	Normal–Abnormal	2 × 5-Fold CV	Ensemble	79.00
10	Proposed scheme	MIAS	Normal–Benign–Malignant	10-Fold CV	Ensemble	91.00

[a]MLP: Multilayer Perception.
[b]NN: Neural Network.

Table 6
A comparison of the proposed scheme and related works applied to the DDSM dataset.

No.	Reference	Dataset	Predicted class	Validation	Classifier	Accuracy (%)
1	Dhahbi et al. (2015)	DDSM	Benign–Malignant	2 × 5-Fold CV	KNN	60.43
2	da Rocha, Junior, Silva, de Paiva, and Gattass (2016)	DDSM	Benign–Malignant	80–20%	SVM	88.31
3	Tsochatzidis et al. (2017)	DDSM	Benign–Malignant	10-Fold CV	SVM	81.00
4	Sapate et al. (2018)	DDSM	Benign–Malignant	10-Fold CV	SVM	87.00
					KNN	85.00
5	Chakraborty et al. (2018)	DDSM	Benign–Malignant	10-Fold CV	RF	77.89
					NB	72.79
6	Al-Antari et al. (2018)	DDSM	Normal–Benign–Malignant	2-Fold CV	DBN[a]	92.86
7	Muramatsu et al. (2020)	DDSM	Benign–Malignant	3-Fold CV	CNN	81.40
8	Lou et al. (2021)	DDSM	Benign–Malignant	3-Fold CV	MGBN[b]	76.99
9	Soulami et al. (2022)	DDSM	Normal–Benign–Malignant	5-Fold CV	CapsNet	77.78
10	Proposed scheme	DDSM	Normal–Benign–Malignant	10-Fold CV	Ensemble	93.26

[a]DBN: Deep Belief Network.
[b]MGBN: Multi-level Global-guided Branch-attention Network.

the average of these metrics, the results of which are respectively shown for MIAS and DDSM data in Fig. 15(a) and (b). Generally, the classification results of the proposed ensemble classifier model in this study surpass the compared classifiers. The average specificity in MIAS data using the KNN classifier is 83.20%. It is evident from Fig. 15(a) that the average specificity of our proposed ensemble classifier was slightly lower (i.e., 0.26%) than that of the KNN classifier. The average specificity in DDSM data using the bagging classifier is 93.49%. In addition, Fig. 15(b) indicates the average specificity of our proposed ensemble classifier was slightly lower (i.e., 0.29%) than that of the bagging classifier. Thus, the proposed classifier not only outperformed its individual components, it was also superior to other commonly used algorithms and, in combination with a feature weighting step, could be effectively applied to assist radiologists in breast cancer detection to reduce the incidence of false positives.

6.5. A comparison of the proposed algorithm with related works

The advantages of the proposed scheme for breast cancer classification were investigated through a comparison with representative works conducted in recent years. Accuracy, the most commonly used evaluation metric for comparing classification results, is provided for both the proposed and conventional algorithms in Tables 5 and 6, for the MIAS and DDSM data, respectively. Several of these existing studies focused on binary classification (i.e., Normal–Abnormal or Benign–Malignant). For example, Shaikh et al. developed a convolutional neural network (CNN) model for the classification of breast cancer (normal and abnormal) (Shaikh et al., 2021), achieving 87.5% accuracy for the MIAS dataset. Alruwaili et al. utilized modified ResNet50 (MOD-RES) and Nasnet-Mobile models to classify mammograms into benign and malignant categories (Alruwaili & Gouda, 2022). MIAS data were further used to verify the effectiveness of this technique, achieving an accuracy of 89.5%. However, multi-classification (i.e., normal, benign, and malignant) is superior to binary classification in helping radiologists diagnose breast cancer, though it presents a distinct set of challenges. In addition, experimental validation data can generally be divided into training and test sets using a proportional division or k-fold CV method, to verify algorithm performance. For example, da Rocha et al. introduced a breast cancer detection strategy based on texture analysis, in which the proportional division method was used to divide DDSM data and evaluate performance (da Rocha et al., 2016). SVM was used to classify the extracted texture features for masses in mammograms as benign or malignant. The highest accuracy (88.31%) was achieved using 80%–20% proportional division. The k-fold CV technique, used in the majority of works shown in Tables 5 and 6, typically achieved more stable and reliable classification results.

In this study, an ensemble classifier model including KNN, bagging, and EigenClass algorithms was developed to determine whether a mammogram included normal, benign, or malignant tumors using a majority voting rule. A 10-fold CV technique was then applied to verify the performance of this strategy using the MIAS and DDSM datasets. Feature weighting based on an improved INFO algorithm was also utilized to assign weights to each feature, further improving the accuracy of classification. As shown in Tables 5 and 6, the average accuracy was 91.00% and 93.26% for MIAS and DDSM data, respectively. The average accuracy of the proposed ensemble classifier is evidently superior to the compared works conducted in recent years. In addition, the proposed scheme was experimentally confirmed to be more effective and reliable.

7. Conclusion

Breast cancer detection is an extremely challenging task for radiologists. This study proposed an automated breast cancer detection scheme for application to mammogram images, utilizing an ensemble classifier

model and a feature weighting algorithm. As a preprocessing step, a novel region extraction method was first proposed using image fusion and filtering techniques to constrain the search area for suspicious breast lesions. These areas offered reliable contour information and high fidelity with little noise. A pectoral muscle removal approach was also proposed to reduce interference and improve the identification of ROIs. Furthermore, an effective segmentation strategy was developed to automatically identify ROIs whose textural and morphological features were fused to generate a feature vector, which was then assigned weights using a feature weighting algorithm. Finally, an ensemble classifier model was proposed to determine whether a mammogram included normal, benign, or malignant tumors using a majority voting rule. In order to verify the effectiveness of the proposed scheme, a sequence of experiments was conducted using the DDSM and MIAS datasets, in which the performance of breast cancer detection was measured by different evaluation metrics (i.e., Acc, Pre, Rec, F-1, and Spe) using a 10-fold cross-validation technique. The average accuracy for the DDSM and MIAS datasets was 93.26% and 91.00%, respectively, demonstrating the proposed scheme outperformed comparable algorithms in recent years. Therefore, the proposed scheme could be highly practical and effective for helping radiologists to detect breast cancer, greatly reducing the incidence of false positives and false negatives.

It is evident there are limitations to the proposed methodology. Firstly, a label or artifact is attached to the breast region, which cannot be removed using the proposed region extraction method. Therefore, we hope region extraction can be improved so as to separate the label or artifact from the breast region. Secondly, the proposed automated ROI segmentation strategy can only select ROIs that are most likely to be lesions. However, there is possibly more than one lesion area in each mammogram. As such, we hope an automated ROI segmentation technique could be developed to detect and segment multiple ROIs. Thirdly, future research will involve further improvements to the proposed strategy, as only textural and morphological ROI features were extracted and input to the ensemble classifier. These features are critical and we intend to utilize a more diverse array of features (such as deep features (Meraj et al., 2021)) in the future, which may further improve diagnostic performance. Fourthly, large breast cancer datasets cannot be employed in the proposed scheme because they are very difficult to obtain when considering patient privacy. A data augmentation technique could potentially be used to address problems with access to big breast cancer datasets in future work. Fifthly, this approach was developed specifically for mammogram images. However, the region extraction technique in this approach is also available for other biomedical imaging modalities (i.e., ultrasound, MR, and histology) to remove noise and enhance the image quality. In a future study, we plan to extend this approach to these and other modalities to screen for breast cancer.

CRediT authorship contribution statement

Fei Yan: Conceptualization, Investigation, Methodology, Funding acquisition, Writing – original draft, Writing – review & editing. **Hesheng Huang:** Methodology, Software, Validation, Data curation, Visualization, Writing – original draft, Writing – review & editing. **Witold Pedrycz:** Investigation, Formal analysis, Supervision, Validation, Writing – review & editing. **Kaoru Hirota:** Formal analysis, Supervision, Validation, Writing – review & editing.

Declaration of competing interest

The authors declare that they have no known competing financial interests or personal relationships that could have appeared to influence the work reported in this paper.

Data availability

The authors are unable or have chosen not to specify which data has been used.

Acknowledgments

This work was supported by the Jilin Provincial Department of Science and Technology, China under Grant 20210201075GX.

References

Ahmadianfar, I., Heidari, A. A., Noshadian, S., Chen, H., & Gandomi, A. H. (2022). INFO: An efficient optimization algorithm based on weighted mean of vectors. *Expert Systems with Applications*, *195*, Article 116516.

Al-Antari, M. A., Al-Masni, M. A., Park, S. U., Park, J., Metwally, M. K., Kadah, Y. M., et al. (2018). An automatic computer-aided diagnosis system for breast cancer in digital mammograms via deep belief network. *Journal of Medical & Biological Engineering*, *38*(3), 443–456.

Aljuaid, H., Alturki, N., Alsubaie, N., Cavallaro, L., & Liotta, A. (2022). Computer-aided diagnosis for breast cancer classification using deep neural networks and transfer learning. *Computer Methods and Programs in Biomedicine*, *223*, Article 106951.

Alruwaili, M., & Gouda, W. (2022). Automated breast cancer detection models based on transfer learning. *Sensors*, *22*(3), Article 876.

Althobaiti, M. M., Ashour, A. A., Alhindi, N. A., Althobaiti, A., Mansour, R. F., Gupta, D., et al. (2022). Deep transfer learning-based breast cancer detection and classification model using photoacoustic multimodal images. *BioMed Research International*, *2022*, Article 3714422.

Assari, Z., Mahloojifar, A., & Ahmadinejad, N. (2022). Discrimination of benign and malignant solid breast masses using deep residual learning-based bimodal computer-aided diagnosis system. *Biomedical Signal Processing and Control*, *73*, Article 103453.

Bray, F., Laversanne, M., Weiderpass, E., & Soerjomataram, I. (2021). The ever-increasing importance of cancer as a leading cause of premature death worldwide. *Cancer*, *127*(16), 3029–3030.

Cao, J., Pang, Y., Xie, J., Khan, F. S., & Shao, L. (2021). From handcrafted to deep features for pedestrian detection: A survey. *IEEE Transactions on Pattern Analysis and Machine Intelligence*, *44*(9), 4913–4934.

Chakraborty, J., Midya, A., & Rabidas, R. (2018). Computer-aided detection and diagnosis of mammographic masses using multi-resolution analysis of oriented tissue patterns. *Expert Systems with Applications*, *99*, 168–179.

da Rocha, S. V., Junior, G. B., Silva, A. C., de Paiva, A. C., & Gattass, M. (2016). Texture analysis of masses malignant in mammograms images using a combined approach of diversity index and local binary patterns distribution. *Expert Systems with Applications*, *66*, 7–19.

Dhahbi, S., Barhoumi, W., & Zagrouba, E. (2015). Breast cancer diagnosis in digitized mammograms using curvelet moments. *Computers in Biology and Medicine*, *64*, 79–90.

Duarte, M. A., Alvarenga, A. V., Azevedo, C. M., Calas, M. J. G., Infantosi, A. F., & Pereira, W. C. (2015). Evaluating geodesic active contours in microcalcifications segmentation on mammograms. *Computer Methods and Programs in Biomedicine*, *122*(3), 304–315.

Erkan, U. (2021). A precise and stable machine learning algorithm: Eigenvalue classification (EigenClass). *Neural Computing and Applications*, *33*(10), 5381–5392.

Escorcia-Gutierrez, J., Mansour, R. F., Beleño, K., Jiménez-Cabas, J., Pérez, M., Madera, N., et al. (2022). Automated deep learning empowered breast cancer diagnosis using biomedical mammogram images. *Computers, Materials and Continua*, (71), 3–4221.

Girija, O. K., & Sudheep, E. M. (2022). Mammogram pectoral muscle removal and classification using histo-sigmoid based ROI clustering and SDNN. *Multimedia Tools and Applications*, *81*(15), 20993–21026.

Gupta, S., Deep, K., Heidari, A. A., Moayedi, H., & Wang, M. (2020). Opposition-based learning harris hawks optimization with advanced transition rules: Principles and analysis. *Expert Systems with Applications*, *158*, Article 113510.

Han, S., Kang, H. K., Jeong, J. Y., Park, M. H., Kim, W., Bang, W. C., et al. (2017). A deep learning framework for supporting the classification of breast lesions in ultrasound images. *Physics in Medicine and Biology*, *62*(19), Article 7714.

Heath, M., Bowyer, K., Kopans, D., Kegelmeyer, P., Moore, R., Chang, K., et al. (1998). Current status of the digital database for screening mammography. In *Digital mammography* (pp. 457–460).

Heidari, M., Mirniaharikandehei, S., Liu, W., Hollingsworth, A. B., Liu, H., & Zheng, B. (2019). Development and assessment of a new global mammographic image feature analysis scheme to predict likelihood of malignant cases. *IEEE Transactions on Medical Imaging*, *39*(4), 1235–1244.

Hovda, T., Hoff, S. R., Larsen, M., Romundstad, L., Sahlberg, K. K., & Hofvind, S. (2022). True and missed interval cancer in organized mammographic screening: A retrospective review study of diagnostic and prior screening mammograms. *Academic Radiology*, *29*, S180–S191.

Joo, S., Yang, Y. S., Moon, W. K., & Kim, H. C. (2004). Computer-aided diagnosis of solid breast nodules: Use of an artificial neural network based on multiple sonographic features. *IEEE Transactions on Medical Imaging*, *23*(10), 1292–1300.

Kilday, J., Palmieri, F., & Fox, M. D. (1993). Classifying mammographic lesions using computerized image analysis. *IEEE Transactions on Medical Imaging*, *12*(4), 664–669.

Larsen, M., Aglen, C. F., Lee, C. I., Hoff, S. R., Lund-Hanssen, H., Lång, K., et al. (2022). Artificial intelligence evaluation of 122 969 mammography examinations from a population-based screening program. *Radiology*, *303*(3), 502–511.

Li, H., Chen, D., Nailon, W. H., Davies, M. E., & Laurenson, D. I. (2021). Dual convolutional neural networks for breast mass segmentation and diagnosis in mammography. *IEEE Transactions on Medical Imaging*, *41*(1), 3–13.

Li, B., Ge, Y., Zhao, Y., Guan, E., & Yan, W. (2018). Benign and malignant mammographic image classification based on convolutional neural networks. In *Proceedings of the 10th international conference on machine learning and computing* (pp. 247–251).

Lin, W., Hasenstab, K., Moura Cunha, G., & Schwartzman, A. (2020). Comparison of handcrafted features and convolutional neural networks for liver MR image adequacy assessment. *Scientific Reports*, *10*(1), 1–11.

Lotter, W., Diab, A. R., Haslam, B., Kim, J. G., Grisot, G., Wu, E., et al. (2021). Robust breast cancer detection in mammography and digital breast tomosynthesis using an annotation-efficient deep learning approach. *Nature Medicine*, *27*(2), 244–249.

Lou, M., Wang, R., Qi, Y., Zhao, W., Xu, C., Meng, J., et al. (2021). MGBN: Convolutional neural networks for automated benign and malignant breast masses classification. *Multimedia Tools and Applications*, *80*(17), 26731–26750.

Mahmood, T., Li, J., Pei, Y., Akhtar, F., Rehman, M. U., & Wasti, S. H. (2022). Breast lesions classifications of mammographic images using a deep convolutional neural network-based approach. *PLoS One*, *17*(1), Article e0263126.

Maqsood, S., Damaševičius, R., & Maskeliūnas, R. (2022). TTCNN: A breast cancer detection and classification towards computer-aided diagnosis using digital mammography in early stages. *Applied Sciences*, *12*(7), Article 3273.

Meraj, T., Alosaimi, W., Alouffi, B., Rauf, H. T., Kumar, S. A., Damaševičius, R., et al. (2021). A quantization assisted U-Net study with ICA and deep features fusion for breast cancer identification using ultrasonic data. *PeerJ Computer Science*, *7*, Article e805.

Milosevic, M., Jankovic, D., & Peulic, A. (2015). Comparative analysis of breast cancer detection in mammograms and thermograms. *Biomedical Engineering/Biomedizinische Technik*, *60*(1), 49–56.

Moghbel, M., Ooi, C. Y., Ismail, N., Hau, Y. W., & Memari, N. (2020). A review of breast boundary and pectoral muscle segmentation methods in computer-aided detection/diagnosis of breast mammography. *Artificial Intelligence Review*, *53*(3), 1873–1918.

Muramatsu, C., Nishio, M., Goto, T., Oiwa, M., Morita, T., Yakami, M., et al. (2020). Improving breast mass classification by shared data with domain transformation using a generative adversarial network. *Computers in Biology and Medicine*, *119*, Article 103698.

Mustra, M., Grgic, M., & Rangayyan, R. M. (2016). Review of recent advances in segmentation of the breast boundary and the pectoral muscle in mammograms. *Medical & Biological Engineering & Computing*, *54*(7), 1003–1024.

Nabizadeh, N., & Kubat, M. (2015). Brain tumors detection and segmentation in MR images: Gabor wavelet vs. statistical features. *Computers & Electrical Engineering*, *45*, 286–301.

Nanglia, S., Ahmad, M., Khan, F. A., & Jhanjhi, N. (2022). An enhanced predictive heterogeneous ensemble model for breast cancer prediction. *Biomedical Signal Processing and Control*, *72*, Article 103279.

Pollesch, N. L., & Dale, V. H. (2016). Normalization in sustainability assessment: Methods and implications. *Ecological Economics*, *130*, 195–208.

Qasem, A., Sheikh Abdullah, S. N. H., Sahran, S., Albashish, D., Goudarzi, S., & Arasaratnam, S. (2022). An improved ensemble pruning for mammogram classification using modified Bees algorithm. *Neural Computing and Applications*, *34*(12), 10093–10116.

Ragab, M., Albukhari, A., Alyami, J., & Mansour, R. F. (2022). Ensemble deep-learning-enabled clinical decision support system for breast cancer diagnosis and classification on ultrasound images. *Biology*, *11*(3), Article 439.

Rampun, A., Morrow, P. J., Scotney, B. W., & Winder, J. (2017). Fully automated breast boundary and pectoral muscle segmentation in mammograms. *Artificial Intelligence in Medicine*, *79*, 28–41.

Rodrigues, E. O., Conci, A., & Liatsis, P. (2020). ELEMENT: Multi-modal retinal vessel segmentation based on a coupled region growing and machine learning approach. *IEEE Journal of Biomedical and Health Informatics*, *24*(12), 3507–3519.

Rouhi, R., & Jafari, M. (2016). Classification of benign and malignant breast tumors based on hybrid level set segmentation. *Expert Systems with Applications*, *46*, 45–59.

Sapate, S. G., Mahajan, A., Talbar, S. N., Sable, N., Desai, S., & Thakur, M. (2018). Radiomics based detection and characterization of suspicious lesions on full field digital mammograms. *Computer Methods and Programs in Biomedicine*, *163*, 1–20.

Sechopoulos, I., Teuwen, J., & Mann, R. (2021). Artificial intelligence for breast cancer detection in mammography and digital breast tomosynthesis: State of the art. *Seminars in Cancer Biology*, *72*, 214–225.

Shaikh, K., Krishnan, S., & Thanki, R. (2021). Deep learning model for classification of breast cancer. In *Proceedings of the artificial intelligence in breast cancer early detection and diagnosis* (pp. 93–100).

Sharma, S., & Khanna, P. (2015). Computer-aided diagnosis of malignant mammograms using Zernike moments and SVM. *Journal of Digital Imaging*, *28*(1), 77–90.

Shen, T., Wang, J., Gou, C., & Wang, F. (2020). Hierarchical fused model with deep learning and type-2 fuzzy learning for breast cancer diagnosis. *IEEE Transactions on Fuzzy Systems*, *28*(12), 3204–3218.

Shivhare, E., & Saxena, V. (2021). Breast cancer diagnosis from mammographic images using optimized feature selection and neural network architecture. *International Journal of Imaging Systems and Technology*, *31*(1), 253–269.

Singh, S. P., & Urooj, S. (2016). An improved CAD system for breast cancer diagnosis based on generalized pseudo-Zernike moment and Ada-DEWNN classifier. *Journal of Medical Systems*, *40*(4), Article 105.

Soulami, K. B., Kaabouch, N., & Saidi, M. N. (2022). Breast cancer: Classification of suspicious regions in digital mammograms based on capsule network. *Biomedical Signal Processing and Control*, *76*, Article 103696.

Suckling, J. (1994). The mammographic images analysis society digital mammogram database. In *Proceedings of the international congress series, vol. 1069* (pp. 375–378).

Sung, H., Ferlay, J., Siegel, R. L., Laversanne, M., Soerjomataram, I., Jemal, A., et al. (2021). Global cancer statistics 2020: GLOBOCAN estimates of incidence and mortality worldwide for 36 cancers in 185 countries. *CA: A Cancer Journal for Clinicians*, *71*(3), 209–249.

Ting, F. F., Tan, Y. J., & Sim, K. S. (2019). Convolutional neural network improvement for breast cancer classification. *Expert Systems with Applications*, *120*, 103–115.

Tripathi, R. K., & Jalal, A. S. (2021). Novel local feature extraction for age invariant face recognition. *Expert Systems with Applications*, *175*, Article 114786.

Tsochatzidis, L., Zagoris, K., Arikidis, N., Karahaliou, A., Costaridou, L., & Pratikakis, I. (2017). Computer-aided diagnosis of mammographic masses based on a supervised content-based image retrieval approach. *Pattern Recognition*, *71*, 106–117.

Wadhwa, A., Bhardwaj, A., & Singh Verma, V. (2019). A review on brain tumor segmentation of MRI images. *Magnetic Resonance Imaging*, *61*, 247–259.

Yan, F., Huang, H., & Yu, X. (2022). A multiwatermarking scheme for verifying medical image integrity and authenticity in the Internet of Medical things. *IEEE Transactions on Industrial Informatics*, *18*, 8885–8894.

Yassin, N. I., Omran, S., El Houby, E. M., & Allam, H. (2018). Machine learning techniques for breast cancer computer aided diagnosis using different image modalities: A systematic review. *Computer Methods and Programs in Biomedicine*, *156*, 25–45.

Zebari, D. A., Ibrahim, D. A., Zeebaree, D. Q., Haron, H., Salih, M. S., Damaševičius, R., et al. (2021a). Systematic review of computing approaches for breast cancer detection based computer aided diagnosis using mammogram images. *Applied Artificial Intelligence*, *35*(15), 2157–2203.

Zebari, D. A., Ibrahim, D. A., Zeebaree, D. Q., Mohammed, M. A., Haron, H., Zebari, N. A., et al. (2021b). Breast cancer detection using mammogram images with improved multi-fractal dimension approach and feature fusion. *Applied Sciences*, *11*(24), Article 12122.